Politecnico di Torino
Belgian Nuclear higher Education Network

Master's Degree in Nuclear Engineering

Master's Degree Thesis

Nuclear data uncertainty quantification in fuel depletion calculations

Promoters

Prof. Sandra DULLA

Prof. Christophe BRUGGEMAN

Mentors

Dr. Pablo ROMOJARO

Dr. Luca FIORITO

Candidate

Federico GRIMALDI

October 2022

Abstract

Spent nuclear fuel characterisation is a topic of major interest in these times of change, when sustainable energy scenarios are shaped. The burden of experimental assessment of spent fuel inventory is too large to allow the application of this technique to all the fuel used in nuclear reactors. For this reason, fuel assembly models capable of predicting the discharged fuel inventory are needed. The validation of such models and of the capabilities of the codes used is often assessed through benchmark modelling. This consists in models of specific fuel assemblies designed following given specifications, which allows for comparison of the model prediction with the results of the experimental campaigns performed on samples from those assemblies, but also for comparison of different modelling codes and of nuclear data libraries.

When it comes to uncertainty propagation, several uncertainty sources should be considered. In the following, after the description and validation of three benchmark models against experimental results, the uncertainty on the cross section data is propagated through such models to the spent fuel inventory. This is done via multivariate statistical sampling, comparing the uncertainty evaluation given by a number of nuclear data libraries.

This thesis highlights the need of continuous improvement on the nuclear data covariance information as well as the relevance of identifying the mechanisms of uncertainty buildup. The uncertainty on the spent nuclear fuel inventory builds up through neutron-induced reactions linking some nuclides' concentrations and their uncertainty, but it also builds up during irradiation according to phenomena whose relevance changes too. Moreover, the weight of those correlations and phenomena is shown to be dependent on the information stored in the nuclear data library considered in the simulation.

Summary

The energy sector is now facing a phase of transition from the fossil fuel to more sustainable options. Therefore, several energy forecasting scenarios are developed [1] and many projects aim at assessing the several options available. In this frame, the characterisation of spent nuclear fuel inventory and of its uncertainty is of key importance and central aim of a number of projects at the European level [2, 3].

The benchmarks of three pressurised water reactors samples — i.e. Calvert Cliffs MKP109-P, Gösgen GU3 and Takahama SF95-4 — were modelled in Serpent to predict the nuclide inventory of samples that were experimentally analysed in international campaigns. A model of Gösgen GU3 was developed in ALEPH too, contributing to the validation of such a code. The developed models were then validated against the experimental results.

The evaluated uncertainty on the cross section of actinides was then propagated through simplified versions of the models to reduce the computational burden of such a study. Several evaluations were considered to do so: ENDF/B-VIII.0 [4], JEFF-3.3 [5], JENDL-4.0u [6] and JEFF-4.0t1 [7]. The uncertainty was predicted via statistical sampling using SANDY [8], to which development a contribution was given in the course of this thesis work.

The main mechanisms of uncertainty buildup were identified and are reported in the comments to the obtained results. The effect of the different evaluations and of the missing covariance data was assessed and reported. The comparative analysis of JEFF-3.3 with JEFF-4.0t1 performed on Gösgen GU3 case study reflects the improvements in terms of the increased number of covariance evaluations. Overall, the uncertainty results were found to be in line with each other for the three different case study considered.

A further investigation on the uncertainty buildup with burnup was performed for Calvert Cliffs MKP109-P and Takahama SF95-4. There, the discrepancies coming from the different evaluations considered and from the different initial enrichment of the two samples were identified. Most of those differences were found to be explained by sensitivity changes during irradiation.

Acknowledgements

The work presented herein was financially supported partially by the Euratom research and training program under the EC H2020 EURAD project (grant agreement ID: 847593). I would also like to acknowledge the Belgian Nuclear higher Education Network (BNEN) where I was an exchange student in the last year in the frame of E+/EU PROGRAMME COUNTRIES mobility program, hosted by the Université de Liège.

I would like to acknowledge my promoters Prof. Christophe Bruggeman and Prof. Sandra Dulla, whose feedback was precious for the speculation on this thesis topic, being specific on the commented results, but always focusing on the broader picture as well.

I would also like to thank my mentor Dr. Ing. Pablo Romojaro and my comentor Dr. Ing. Luca Fiorito. They made this work possible guiding me in the physical understanding of the presented phenomena. Their advice carried me through the stages of this project. Thank you also to the members of NSP and NSM groups at SCK CEN, who created a stimulating work environment and provided me with many interesting feedback on this work.

Finally, I would like to thank my family and friends whose sometimes hidden contribution to this degree was of major value. Among them, a special thank goes to Samuele Corona, Eleonora Agus and Enrica Belfiore, who shared with me the many ups and downs of the last five years, and to those who directly or indirectly contributed to the moments of joy of my stay in Belgium.

Table of Contents

List of Tables

List of Figures

Acronyms

ANOVA

Analysis of variance

API

Application Programming Interface

BWR

Boiling water reactor

CLT

Central limit theorem

C/C-1

Comparison of calculated results under. It is often used to compare the results of a simplified calculation (numerator) with the one of a more accurate one (denominator). C/C-1 can also refer to the comparison of the results of two different models, such as in 3.2.3, where this form is used to compare the results of Serpent model (numerator) with the ones of ALEPH model (denominator).

C/E-1

Comparison of experimental results and calculated ones. C is the calculated result and E the experimental one.

DA

Destructive analysis

E/C-1

Comparison of experimental results and calculated ones. C is the calculated result and E the experimental one.

GEN III+

generation "three-plus"

GEN IV

generation "four"

İTÜ

İTÜ Energy Institute

JAERI

Japan Atomic Energy Research Institute

KRI

Khlopin Radium Institute

LWR

Light water reactor

MC

Monte Carlo

MOX

Mixed Oxide fuel

NDA

Non-destructive analysis

NPP

Nuclear Power Plant(s)

ORNL

Oak Ridge National Laboratory

PNL

Pacific Northwest Laboratory

PWR

Pressurised water reactor

RAM

Random access memory

RIM

Radiation induced damage in nuclear materials

SANDY

SAmpler of Nuclear Data uncertaintY

SCK CEN

Belgian nuclear research center

SNF

Spent Nuclear Fuel

TMC

Total Monte Carlo

Chapter 1

Introduction

1.1 Motivation

Energy forecasting scenarios consider nuclear technologies among the relevant alternatives to fossil fuels [1]. Moreover, IAEA [9] reports more than 390 GW electrical capacity installed worldwide. For these reasons, technological problems posed by nuclear technologies are much related to present and future energy production scenarios. Their tackling is a key effort whose success can define and shape energy production means for years to come.

Nuclear power plants provide the possibility to install large capacities and guarantee almost continuous power production. Moreover, more advanced and even safer technologies are now being developed and deployed — i.e. GEN III+ and GEN IV ones. Despite this, nuclear power plants (NPPs) also have risks related to activated materials and fuel handling, among the others. In this frame, and considering the importance of sustainability, spent nuclear fuel (SNF) characterisation is a subject of interest to which European projects are devoting efforts, such as EURAD [2] in the context of Horizon 2020 [3].

Following these considerations, the nuclide composition of SNF is relevant as it is the inherent source of risk in SNF (more details on this in section 1.2). SNF inventory knowledge can provide designers with more accurate input parameters to design safe and efficient transportation casks, temporary deposits for SNF as well as long term and final disposals. SNF inventory is also relevant when thinking of technologies and processes aiming at closing the nuclear fuel cycle, either via fuel reprocessing to mixed oxides one (MOX) or via partitioning and transmutation projects.

Clarified the needs to know the SNF composition, the focus shifts to another related question: *«How precise should the information on SNF inventory be?»* Given the technological orientation of many of the work groups focused on this,

which are often aiming at facility design, the target uncertainty requirements are often reported in terms of uncertainties on specific integral observables, rather than in terms of uncertainties on the SNF composition.

Before entering a more detailed discussion on the differences in considering SNF composition uncertainties and observable-oriented ones, which is done in section 1.2, two examples on the context of the impact in the uncertainty are mentioned. One qualitative example on the needs to have clear uncertainty quantification of SNF inventory comes from the MOX fuel cycle. There, ^{238}Pu presence limits the process as its half life (around 88 y, which is short compared to the other plutonium isotopes) and its branching ratio (100% α decay) result in radiation protection needs and in heat generation during the fuel reprocessing process. Such a design constraint is to be respected also considering the uncertainties on the ^{238}Pu content, that is on SNF content, generalising the discussion to other applications. This highlights the need to adequately assess the uncertainty in the calculated SNF inventory.

The second example reported is more related to the economical context of the fuel cycle and more specifically of the SNF disposal. As a matter of fact, many countries in Europe and worldwide are designing long term disposal facilities for their high level nuclear waste. Among them, Finland is developing the design of a facility for SNF disposal to be located in Onkalo. Considering the data reported in Ref. [10], the operational cost will be approximately 330 000 $\frac{\$}{\text{container}}$ while the total cost will be about 610 000 $\frac{\$}{\text{container}}$ in 2009 prices. For this reason, an improvement on the design or on the side of nuclide inventory knowledge that would result in even a 1% cost reduction, will be worth about 3 to 6 $\frac{\text{k}\$}{\text{container}}$ saving, resulting in a total saving of 9 - 17 M$, order of magnitude. More figures on the cost of radioactive waste disposal are reported in Ref. [11]. This case was reported to reflect the economical benefit that could result from a better description of SNF inventory, as even if relative improvement values might look small, their effect on economical savings can be of major relevance.

1.2 Nuclides of interest for spent nuclear fuel characterisation

As mentioned, not all nuclides present in SNF contribute the same way to radiological risk, radio-toxicity and to design constraint definition. $\alpha-$, $\beta-$ or $\gamma-$emitters, or nuclides that are progenitors to those nuclides, are typically of major importance for safety considerations on SNF composition. Also nuclides that undergo spontaneous fission are relevant both for the dose they can deposit in the surrounding structures — which can also affect the personnel handling the SNF — and for their contribution to SNF reactivity. Moreover, since the inventory of SNF changes in

time, so does the contribution to the observables of the many nuclides present in SNF. This is because the considered time scales for such physical problems are the ones of the half lives of the nuclides involved, which vary from fractions of seconds to millions of years.

For these reasons, not all nuclides shall then be taken in the same consideration in SNF characterisation. As a matter of fact, references in the field reporting experimental analyses results focus on specific nuclides that proved to be the major contributors to the above described risks [12, 13, 14]. According to this, the presented thesis focuses on a selected set of nuclides, resulting from a combination of the ones relevant for SNF analysis with the ones relevant for the reactor control and the ones included in the considered benchmark experiments.

The uncertainty on the SNF inventory relates to the one on the observables as in TAB. 1.1, where several relations are reported. There, p_r, s_γ and s_n respectively indicate the decay heat, γ emission rate spectrum density and neutron emission rate densities, as well as $s_{SF,i}$ and $s_{\alpha,i}$, that are the spontaneous fission and α emission rate densities. Also, in TAB. 1.1, λ_i are the decay constants of the $i-$th nuclides, P are the probabilities for a certain emission to happen, possibly at a certain energy E. Therefore, TAB. 1.1 highlights the relations to propagate the uncertainty from the nuclide densities N_i to the SNF observables. This calculation is left out of the scope of this thesis.

Table 1.1: Observables relation with SNF composition

Observable	Equation
Decay heat	$p_r = \Sigma_i E_{ri} \lambda_i N_i$
γ emission	$s_\gamma = \Sigma_{i,j} P_\gamma(E_{\gamma,ij}) \delta(E - E_{\gamma,ij}) \lambda_i N_i$
Neutron emission	$s_n = \Sigma_i (s_{SF,i} + s_{\alpha,i}) N_i$

Several observables have been identified to be of interest in the framework of EURAD [2], which is also the scope in which this thesis works was developed:

- Decay heat (and γ emission);
- Neutron emission;
- Reactivity (fissioning nuclides and nuclides with large absorption cross section);
- Fissile material (Nuclear Safeguards limits);
- Specific long-lived radionuclides for long term safety.

Among the many nuclides contributing to these observables with different relevance and different time scales, a subset was identified based on a literature

search [15, 16, 17, 18, 19, 20, 21]. Thus, the thesis will focus on reporting the concentration in the SNF of the nuclides presented in Tab. 1.2, while the nuclides considered in the experimental assessment of the considered samples will be analysed for the validation of the models. For the sake of comparison, some nuclides whose concentration was not experimentally assessed were considered in the uncertainty analysis, for example in section 4.3.

Table 1.2: Nuclides of interest for SNF inventory

Decay heat	n emission	Reactivity	Fissile	Long-lived
^{90}Sr	^{240}Pu	^{99}Tc	^{235}U	^{36}Cl
^{106}Ru	^{242}Pu	^{235}U	^{238}U	^{79}Se
^{134}Cs	^{242}Cm	^{238}U	^{239}Pu	^{99}Tc
^{137}Cs	^{244}Cm	^{239}Pu	^{241}Pu	^{129}I
^{144}Ce	^{246}Cm	^{240}Pu		
^{154}Eu		^{241}Pu		

1.3 Objectives

Considering the importance of uncertainty quantification of SNF composition and the interest in this topic both from a safety-legislative perspective and from an academic point of view, this thesis aims at assessing a methodology for such an analysis and at using it to propagate the nuclear data uncertainty through three benchmark models, namely the ones based on Calvert Cliffs unit 1, assembly D047, rod MKP109, sample P, Gösgen Ariane GU3, Takahama unit 3, assembly NT3G23, rod SF95, sample 4.

These case studies were chosen for their relevance in the EURAD project and because they allow for comparison of the calculated results to the ones measured in several experimental campaigns. This comparison is an added value to this study, whose focus remains on the uncertainty propagation, as it allows to verify the accuracy of the models developed. Moreover, a clear reference on the best estimate values emphasizes that, despite the uncertainty analysis being the main focus of this work, the concentration of the nuclides which influences the observables is part of the reported results relevant for the many technological applications mentioned. In other words, just like the nuclear data are evaluated as best estimates and uncertainties, also the results of this analysis are reported in the same form.

In the end, given the benchmark nature of the chosen case studies, some considerations on the state of the analysed evaluated nuclear data libraries in terms of best estimates and uncertainty evaluation will be reported. This locates the

thesis in the field of those studies that close the cycle of the evaluation process, returning information on the state of the nuclear data libraries to the evaluators themselves and highlighting where improvement might be needed.

In other words, this thesis aims at performing nuclear data uncertainty propagation through Monte Carlo (MC) codes to the SNF composition and at understanding the phenomena through which such an uncertainty is propagated. This is done both to report to the nuclear data community about the current state of some of the most used nuclear data libraries and to validate both the models and the nuclear data libraries for fuel depletion calculations. With this respect, the results of this work are to be considered in the broader context of SNF uncertainty quantification partially reported in [22, 23, 24, 25, 26, 27, 28, 29, 30, 31].

1.4 Structure

After this brief introduction on the background of this thesis and on its context, the work developed will be presented as follows. First the theoretical background in terms of nuclear physics and transport theory will be briefly summarised in section 2.1 to report which equations were solved to get the presented results. A discussion will be reported on global and local sensitivity analysis, with particular attention to the differences between the two of them, in section 2.2. After that, some considerations on uncertainty and on its propagation through statistical sampling will be reported in sections 2.3 and 2.4. Then an overview of the tools employed in the course of the thesis will be given in sections 2.5 and 2.6.

After the context is shaped, the detailed description of the three modelled assemblies for the relevant irradiation samples will be reported. There, in chapter 3, the comparison of the model results with the experimental ones is reported, as well as an analysis of the bias introduced by some necessary model simplifications.

Chapter 4 is devoted to uncertainty analysis. It starts with some considerations applicable to all the samples. Then the results obtained for Calvert Cliffs MKP109-P, Gösgen GU3 and Takahama SF95-4 samples are reported.

Finally, an analysis of the uncertainty buildup with burnup is carried out in section 4.4 as a complement of what was discussed for Calvert Cliffs MKP109-P and Takahama SF95-4. The conclusions of this work are then summarised in chapter 5, where some future work perspectives are also reported.

Chapter 2

Theoretical background and methodology

2.1 Neutron transport and nuclear fuel transmutation

In this section, the basic phenomenological and physical aspects of the subject of this work are reported. Around what is discussed in the following, the whole work is developed both in terms of methodology and of interpretation of the results.

2.1.1 Neutron-matter interaction

Neutrons are neutral nucleons that compose the nucleus together with protons, which are instead positively charged. Both neutrons and protons can also move freely, without being compounded in atomic nuclei, as they can be generated by sources. Neutron sources can be designed based on several different physical phenomena, among which spontaneous fissions — such as ^{252}Cf — and (α, n) reactions — such as $^{241}\mathrm{Am}(\alpha, n)^{9}\mathrm{Be}$ — should be mentioned [32, 33].

When freely flying, neutrons can then interact with matter. The interaction probability is represented by the microscopic cross section σ for a certain interaction type i, $\sigma_i(E)$, which is dependent on the energy and on the material of the target. When it comes to neutron-matter interaction, reaction i can either be absorption (σ_a), capture (σ_c), fission (σ_f), elastic scattering (σ_{es}), inelastic scattering (σ_{is}), or any other neutron induced reaction, such as $(n, 2n)$ reactions. These reactions relate to each other as follows:

$$\sigma_a = \sigma_f + \sigma_c \qquad \sigma_s = \sigma_{es} + \sigma_{is} \qquad \sigma_t = \sigma_a + \sigma_s, \tag{2.1}$$

where σ_t is the total neutron cross section.

When the neutron is flying in a three-dimensional volume, it is also of interest to define a macroscopic cross section of interaction $\Sigma_i\left(\overrightarrow{r}, E\right)$, which is the probability of interaction per unit path of the neutron:

$$\Sigma_i\left(\overrightarrow{r}, E\right) = N_j\left(\overrightarrow{r}\right)\sigma_i\left(E\right),$$

where $\overrightarrow{r}$ is the volume and N_j is the nuclear density of target material j. The same relations reported in Eq. (2.1) hold for the macroscopic cross section. The inverse of $\Sigma_i\left(\overrightarrow{r}, E\right)$, $\lambda_i\left(\overrightarrow{r}, E\right)$, is the neutron mean free path in the medium.

2.1.2 Neutron transport

The time-balance of neutron density in a volume, at a certain energy and moving along a certain direction,

$$\begin{aligned}\nabla\cdot\left(\overrightarrow{\Omega}\phi\left(\overrightarrow{r}, E, \overrightarrow{\Omega}, t\right)\right)dEd\Omega - \Sigma_t\left(\overrightarrow{r}, E\right)\phi\left(\overrightarrow{r}, E, \overrightarrow{\Omega}, t\right)d\overrightarrow{r}dEd\Omega + \\ + \int d\Omega'\int dE'\Sigma_s\left(\overrightarrow{r}, E'\right)\phi\left(\overrightarrow{r}, E', \overrightarrow{\Omega'}, t\right)f_s\left(\overrightarrow{r}, E'\to E, \overrightarrow{\Omega'}\to\overrightarrow{\Omega}\right)d\overrightarrow{r}dEd\Omega + \\ + S\left(\overrightarrow{r}, E, \overrightarrow{\Omega}, t\right)d\overrightarrow{r}dEd\Omega = \frac{1}{v}\frac{\partial}{\partial t}\left[\phi\left(\overrightarrow{r}, E, \overrightarrow{\Omega}, t\right)\right]d\overrightarrow{r}dEd\Omega \quad (2.2)\end{aligned}$$

can be conceptually expressed as

$$\begin{aligned}&\underset{\text{I. Deterministic}}{\text{(Entering} - \text{Exiting)}} - \underset{\text{II. Statistical}}{\text{Removal}} \pm \underset{\text{III. Statistical}}{\text{Scattering}} + \underset{\text{IV. Source or fission}}{\text{Production}} = \\ &= \underset{\text{V. Deterministic}}{\text{Time Variation}}, \quad (2.3)\end{aligned}$$

following Ref. [34]. In Eq. (2.3), the terms are divided in deterministic and statistical and numbered to ease their separate definition. Such definitions are reported in Tab. 2.1, where the neutron transport equation Eq. (2.2) is commented term by term in its time-integrated form.

In Tab. 2.1, $\overrightarrow{r}$ indicates the volume, E the energy, $\overrightarrow{\Omega}$ the direction and t the time. Moreover, ϕ is the neutron flux and S the intensity of the source, while Σ_i indicates the macroscopic cross section for interaction i. The same notation holds for Eq. (2.2). Two considerations are also worth mentioning. On the one hand, when interpreting the physical meaning of the neutron transport equation, the terms neutron and neutrons will be used interchangeably: the equation has

Table 2.1: Terms of the neutron transport equation

Term	Formulation	Interpretation insights
I	$\nabla \cdot \left(\overrightarrow{\Omega}\phi\left(\overrightarrow{r}, E, \overrightarrow{\Omega}, t\right)\right) dEd\Omega dt$	Application of Gauss and Green's Theorem;
II	$\Sigma_t\left(\overrightarrow{r}, E\right)\phi\left(\overrightarrow{r}, E, \overrightarrow{\Omega}, t\right) d\overrightarrow{r}dEd\Omega dt$	Interaction probability per unit length times neutron path in $[t, t+dt]$;
III	$\int d\Omega' \int dE' \Sigma_s\left(\overrightarrow{r}, E'\right)\phi\left(\overrightarrow{r}, E', \overrightarrow{\Omega'}, t\right) f_s\left(\overrightarrow{r}, E' \to E, \overrightarrow{\Omega'} \to \overrightarrow{\Omega}\right) d\overrightarrow{r}dEd\Omega dt$	Probability to be scattered for any energy E' and direction $\overrightarrow{\Omega'}$ to energy E and direction $\overrightarrow{\Omega}$ of the balance, computed as convolution of the scattering probability density function f_s and of the interaction probability — i.e. probability per unit length times neutron path in $[t, t+dt]$;
IV	$S\left(\overrightarrow{r}, E, \overrightarrow{\Omega}, t\right) d\overrightarrow{r}dEd\Omega dt$	Neutron emission space density within a certain energy and direction range and time interval;
V	$\frac{1}{v}\left[\phi\left(\overrightarrow{r}, E, \overrightarrow{\Omega}, t+dt\right) - \phi\left(\overrightarrow{r}, E, \overrightarrow{\Omega}, t\right)\right] d\overrightarrow{r}dEd\Omega$	Neutron density $\left(n = \frac{1}{v}\phi\right)$ time balance in the volume $d\overrightarrow{r}$ and in dE and $d\Omega$ energy and velocity ranges.

statistical terms, which require a large number of particles to be meaningful; still, thinking of one single neutron is often easier and does not change the overall meaning of the equation. On the other hand, one should notice that the direction $\overrightarrow{\Omega}$ is a vector, while its differential $d\Omega$ is not. This is because $d\Omega$ rather represents the infinitesimal area around $\overrightarrow{\Omega}$, which is a scalar by definition.

In the discussion so far, the fission term of the neutron transport equation was not reported. It can be included in the equation either complementing the source — i.e. as an other positive term to the neutron balance — or as an alternative to it. The latter is often the case for nuclear reactor applications as one wants the fissions to completely compensate for the neutron leakage. For this reason, the fission term is reported as an alternative to the source term in Eq. (2.3). Either case, the fission term is defined as

$$\int d\Omega' \int dE' \Sigma_f \left(\overrightarrow{r}, E'\right) \phi \left(\overrightarrow{r}, E', \overrightarrow{\Omega}', t\right) \frac{\chi\left(\overrightarrow{r}, E\right)}{4\pi} \nu \left(\overrightarrow{r}, E'\right) d\overrightarrow{r}\, dE d\Omega, \tag{2.4}$$

where $\chi\left(\overrightarrow{r}, E\right)$ is the isotropic fission spectrum and E' and $\overrightarrow{\Omega}'$ refer to the neutron energy and direction before the fission (whereas they were the neutron energy and direction after the scattering in Tab. 2.1). This is because one should consider the fissions happening in the volume and time interval induced by neutrons at any energy E' and direction $\overrightarrow{\Omega}'$. The term reported in Eq. (2.4) is therefore consistent in notation to what has been discussed so far. In Eq. (2.4), $\chi\left(\overrightarrow{r}, E\right)$ is then the probability per unit energy to release neutrons at energy E as a consequence of fission, while $\nu\left(\overrightarrow{r}, E'\right)$ is the number of neutrons emitted after a fission taking taking place at energy E'.

Now that the terms involved have been discussed, a smoother notation is included to simplify the phenomenological understanding of the equations. This consists of the definition of the fission operator $\hat{\mathrm{F}}$ and of the leakage operator $\hat{\mathrm{L}}$ as well as of the eigen-formulation of the equation, imposing the fissions to compensate for the leakage and considering no neutron source. This simplified notation results in

$$\hat{\mathrm{L}}\phi\left(\overrightarrow{r}, E, \overrightarrow{\Omega}\right) = \frac{1}{k}\hat{\mathrm{F}}\phi\left(\overrightarrow{r}, E, \overrightarrow{\Omega}\right)$$

for the steady state form of Eq. (2.2) where the fission term was included instead of the source one.

2.1.3 Depletion equation

The nuclear fuel composition evolves in time because of two main phenomena: irradiation-induced transmutation and radioactive decay. Both these processes are included in Eq. (2.5), the Bateman equation [35]. There, the decays of each generic

j nuclide to i are accounted for by the decay constant $\lambda_{j\to i}$, as well as the neutron induced transmutations are represented by their probability $\sigma_{j\to i}$ (or vice versa). Also the decays of nuclide i are considered by λ_i as well as its production by fission, being its fission yield γ_i. In Eq. (2.5), φ refers to the neutron flux shape, while $C(P)$ is the amplitude of the neutron flux. As a matter of fact, the normalised neutron flux $\phi = C(P)\varphi$ has amplitude $C(P)$ that is function of the reactor power, which in turn is proportional to the number of fission (and capture) reactions.

$$\frac{\partial N_i}{\partial t} = \\ = C(P)\sum_j \varphi N_j \sigma_{j\to i} + C(P)\sum_f \varphi N_f \sigma_f \gamma_i + \sum_j N_j \lambda_{j\to i} + \\ - C(P)\sum_j \varphi N_i \sigma_{i\to j} - \sum_i N_i \lambda_i \quad (2.5)$$

Eq. (2.5) results in a set of equations when considering all the i-th nuclides present in a nuclear reactor. This set of equations can be written in the form of a matrix and its solution requires numerical schemes due to the coupling with all the j-th equations.

2.1.4 Solution scheme

The two problems expressed in sections 2.1.2 and 2.1.3 need then to be coupled as the neutron flux causes transmutations modifying the nuclide inventory in the reactor, which in turns affects the neutron flux. The time coupling is therefore often solved by separation of spatial and temporal components of the solution. The neutron flux is evaluated via MC simulation at a certain time, then it is approximated to be constant for a depletion step, during which Eq. (2.5) is numerically solved; then a new neutron flux is estimated considering the updated nuclide inventory in the reactor.

2.2 Global and local sensitivity analysis

When in need to define a methodology to assess the effect of a change in some model input parameter on some the output, perturbation theory can be considered. The key idea behind perturbation theory is to consider a small change of the selected input parameter and to analyse its effect on the output of interest, via analytical calculation or simulation.

Perturbation theory can be of first order or of higher order. The first order perturbation theory presents a key parameter that will be referenced in the following

for the simplicity in which it expresses a deep meaning. This is the sensitivity S of an observable ω_j to an input parameter ξ_i, defined as

$$S_{j,i} = \frac{\delta\omega_j/\omega_j}{\delta\xi_i/\xi_i}$$

In Eq. (2.2), δ indicates a small change in a parameter, meaning a perturbation of ω_j and of ξ_i respectively. In a perspective closer to the application, ω_j could be considered to be the reactor response and ξ_i would be the nuclear data vector.

The sensitivity allows one to reduce the complexity of the model, substituting it with a linear approximation, that is indeed the linear model with the sensitivities multiplying the inputs, as in equation Eq. (2.6), for a model with N input parameters and M outputs.

$$\begin{aligned}
\omega_1 &= \sum_i^N S_{1,i}\xi_i \\
\omega_2 &= \sum_i^N S_{2,i}\xi_i \\
\omega_j &= \sum_i^N S_{j,i}\xi_i \\
\omega_M &= \sum_i^N S_{M,i}\xi_i
\end{aligned} \tag{2.6}$$

Sensitivity is a local measure as it refers to a small perturbation $\delta\eta$ around an expected value η. This is indeed not far from a first order Taylor expansion of the model $\overrightarrow{\omega} = f(\overrightarrow{\xi})$, eventually computed via successive model simulations with perturbed input parameters on which a linear interpolation is then computed to retrieve the sensitivity coefficients.

When analysing the perturbation of an input parameter in the range of its uncertainty to propagate this to the output uncertainty, the validity of the linear approximation should be assessed. This is because the uncertainty of the parameter might be such that the perturbation would not be *local* anymore. To avoid this, considering that often in the cases analysed within this thesis the uncertainty can be large — being the evaluated uncertainty on some cross section of the order of 1000% in certain energy ranges —, a global approach is attempted. This consists in assuming a gaussian distribution for the inputs as the range of possible variation. Then, with successive model instances, the output distribution is assessed and its standard deviation serves as a measure of the output spread, namely of its uncertainty. This idea is behind what is discussed in section 2.4, where more details on the approach to this problem considered in this work are given.

2.3 Contributions to the uncertainty

As mentioned in section 1.3, SNF inventory is not relevant by itself without proper uncertainty quantification. This is needed as it complements the information given by the best estimate coupling it with a reliability quantification; but also, from a more technological point of view, it is relevant to verify and properly establish the many safety margins foreseen for the nuclear installations. To perform uncertainty analysis, detailed investigation of the uncertainty sources should be carried out a priori.

In order to properly perform uncertainty propagation, the model boundaries should be clearly defined. This is because it is necessary to assess which are the inputs and what is their uncertainty as well as the nature of the investigated output before proceeding. Moreover, the assumptions taken in the model design should all be considered with the bias they induce on the output. Therefore, *model* should be considered to be whatever stands between raw input data and results, meaning that each assumption taken in the process — even those related to input and output parameter processing — should be considered as uncertainty source as it introduces a bias in the calculation. Uncertainty quantification from such sources is not straight forward and comparison among different model designs would be required to assess its contribution to total output uncertainty. Such a comparison would require an assessment of the bias introduced by both models as well as of the relative bias to be complete, which makes it too complex. The main uncertainty sources can be identified as:

- nuclear data (cross sections, decay data, fission yields, etc.);
- operational history (such as working temperatures, reactor power levels, boron concentration in the moderator, etc.);
- fuel fabrication (assembly pitch, fuel pin radius, etc.);
- modelling assumptions (sampling distribution, physics simplifications, discretisation, statistical and numerical error, etc.);

among the others.

This work specifically aims at uncertainty propagation from nuclear data to SNF nuclide concentration, basically leaving out of the scope the other reported uncertainty sources. Such an uncertainty propagation can be done quite precisely through statistical sampling. This makes statistical sampling part of the *model* used for uncertainty propagation, meaning it introduces a bias which should be assessed. This is out of the scope of this work, and only few comments are reported on it.

First of all, statistical sampling needs covariance matrices and best estimate values to be implemented, as described in section 2.4. These were taken from the evaluated nuclear data libraries. Lack of information in the evaluated nuclear data libraries is not compensated by any mean, meaning no covariance matrix evaluation is equivalent to no uncertainty on that parameter. The effect of this is commented in detail in chapter 4.

Statistical sampling also implies the choice of a sampling distribution when it is done from the evaluated covariance matrices rather than with total Monte Carlo (TMC) [22, 36], as it is the case in the frame of this work. Usually, and in the following as well, normal distributions are assumed for the sampled input parameters. This choice is justified by the central limit theorem (CLT) and by considerations on the maximum entropy of the distribution. Such a sampling might result in negative sampled values — more likely to appear as the uncertainty on the input parameter grows —, which are often non-physical for nuclear data such as the cross sections and the fission yields. This leads to the need of handling the negative tails of the gaussian distribution. In order to preserve the distribution symmetry, this can be done via re-sampling of the negative samples — and symmetrically the ones larger than twice the distribution mean —, setting the same samples to the mean or setting them to zero or to twice the mean, depending on if they were negative or not. All of these methods result in a reduction of the evaluated uncertainty on the input parameter, which effect should be assessed. This effect is of course more relevant the larger the standard deviation of the distribution. The latter handling was considered developing this thesis as it is the one that affects the distribution standard deviation the less. Some studies (Refs. [37, 38]) propose sampling of the input parameters from lognormal distributions, which are the positive distributions with the largest entropy and which have the advantage of converging to normal distributions when low standard deviations are considered. Further analysis on this should be carried out and is left for future works.

Also, statistical sampling implies the choice of the number of samples to take according to the chosen distribution. This is not trivial and affects the description of the uncertainty of the sampled parameter. To partially verify the adequateness of the chosen number of samples, a convergence study of its mean to the parameter best estimate was carried out. Some examples are reported in Fig. 2.1, where the perturbation coefficient average is presented (more on the relation between perturbation coefficients and nuclear data samples in section 2.6.3).

Among the nuclear data, the cross sections are reported to be the most relevant in terms of SNF inventory as the uncertainties on fission yields were often found to be too high to carry any information and the decay data uncertainty was propagated and proved to be negligible with respect to the one from the cross sections, as reported in Refs. [39, 25]. For this reason, this thesis will focus on cross section uncertainty propagation.

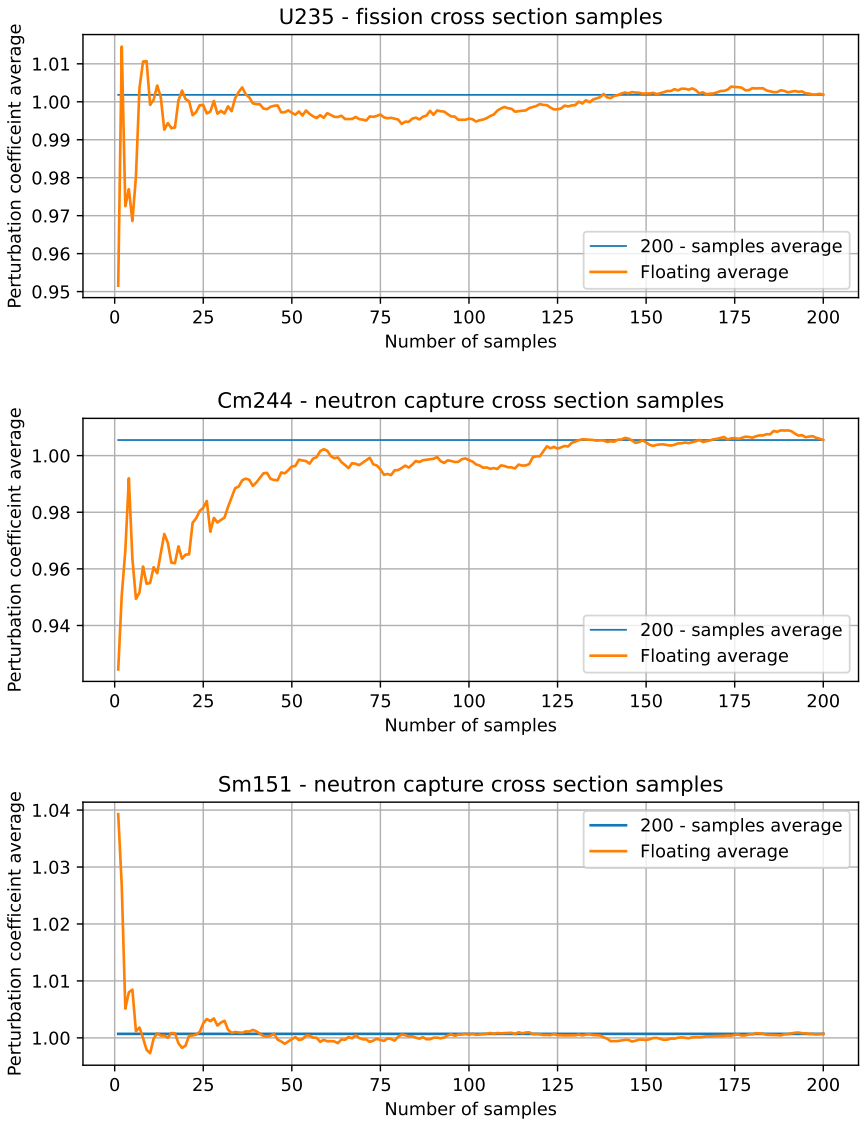

Figure 2.1: Sample average convergence against number of considered samples

In the following, where not explicitly mentioned differently, one single standard deviation is considered to be the uncertainty both for the nuclear data and for the model results. Moreover, in order not to create confusion in the notation, u is used to refer to the uncertainty — i.e. one standard deviation — while σ is left for the microscopic cross section.

2.4 Uncertainty propagation and statistical sampling

In this section, the procedure of statistical sampling is described. The principle behind statistical sampling is fairly simple: considering a set of model input parameters, given with best estimate values and covariance matrices, random values are sampled according to the multivariate assumed distribution characterised by the parameters best estimate values and covariance matrices. Each multivariate sampling results in a sampled set of random values for each parameter, which serves as input for an instance of the model. Repeating the sampling N times and running the model consequently results in N estimations of the model results. The best estimates of the model results will be the results of the calculation fed with the best estimate values of the parameters, while their uncertainties will be the standard deviations over the N results.

A simple implementation of the statistical sampling procedure is represented in Fig. 2.2. There the input parameter is sampled according to a normal distribution — not multivariate in this simple case. The considered samples result in as many dots in the plot, that are the model results with each of the randomly sampled values of the input parameter. Then a distribution is derived from the model outputs and the standard deviation of their set is considered to be the uncertainty on the output.

The complexity of statistical sampling comes with the number of considered input and output parameters. When more than one input is considered, the visualisation reported in Fig. 2.2 is not bi-dimensional anymore and the input sampling distribution is multivariate — i.e. multi-dimensional. Still, the insights from the discussion on Fig. 2.2 can be extrapolated to the more complex cases.

Statistical sampling is therefore inherently global as a perturbation scheme, as the sampling procedure takes into account all the possible input values, just sampled according to a distribution giving them different likelihood to be sampled.

As discussed in section 2.2, local sensitivity consists of a linearisation of the model in the vicinity of a certain best estimate value. The slope of this linearised model is then the sensitivity of the model output to the perturbed model input. To get an equivalent measure of the sensitivity of the output to an input in the context of statistical sampling, linear fitting of the output set can be performed. Sticking to

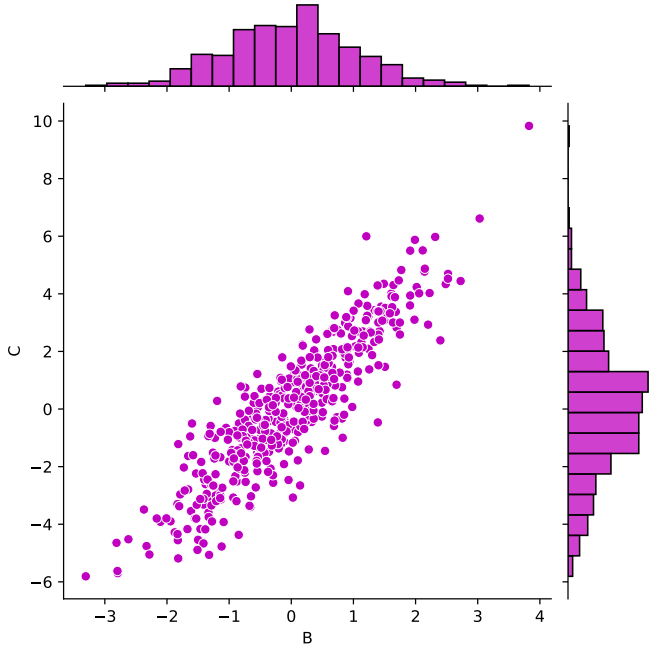

Figure 2.2: Statistical sampling example - B and C are general parameters of the model C = A + 2B, where both A and B were normally sampled.

the non-multivariate case, this results in what is reported in Fig. 2.3. There, two measures are reported: on the one hand, the slope of the fitting line is equivalent to the local sensitivity coefficient, just extrapolated to the global sampling context, while the R^2 parameter is a measure of the share of the output variance that is represented by the linear model. This is both a measure of the correctness of the first order approximation, but also of how relevant the input parameter is in terms of its contribution to the output variance in the linear approximation.

Again, this can be extrapolated to multivariate sampling distribution cases — i.e. computing multivariate linear regression —, where the R^2 parameter representation of the contribution of the input (or set of inputs) to the total output variance is somewhat a measure of the relevance of that input (or set of inputs) for the output. This makes the slope of the fit and R^2 suitable measures of the sensitivity of the output to the input (or set of inputs) under investigation.

2.5 Nuclear data libraries

In order to simulate the physical problems mentioned so far and described by Eqs. (2.2 and 2.5), a set of input data is needed, which knowledge affects the calculation results [40, 19]. Nuclear data are often reported in evaluated nuclear

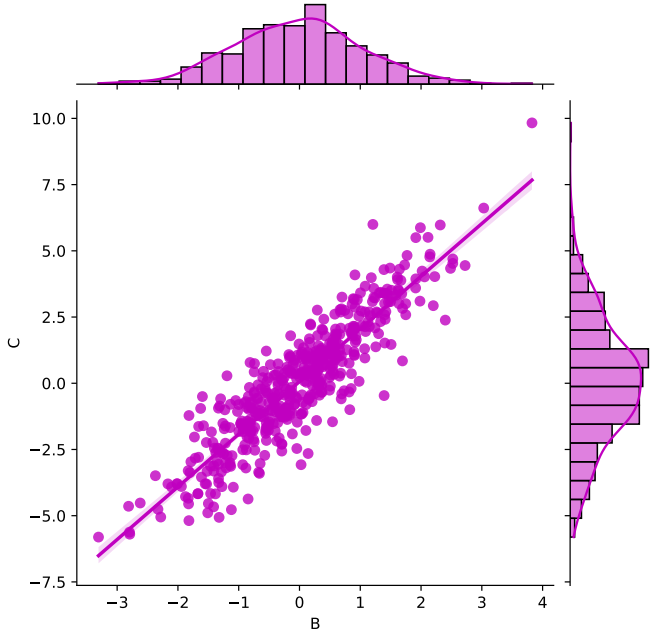

Figure 2.3: Statistical sampling example with linear regression - B and C are general parameters of the model C = A + 2B, where both A and B were normally sampled.

data libraries. Since all the nuclear data used developing this thesis work come from evaluated nuclear data libraries and considering that the differences among several evaluated nuclear data libraries will be reported, this section briefly describes the evaluation process.

The evaluation process is schematised in Fig. 2.4. It starts with tailored experimental campaigns that complement what is already reported in the experimental databases. This results in a data-set of measured nuclear data and experimental uncertainties. These data go through the evaluation process, meaning that they are grouped and eventually complemented with results from physical models. When a set of evaluated nuclear data is ready for the first release, it is made available to the users in the form of an alpha version of the library. This is used in simulations of benchmark models designed on case studies for which experiments were also be performed. The results of these models are then compared with the experimental ones in order to assess the bias introduced by the evaluated nuclear data. Discrepancies or inconsistencies, but also the potential effect of missing evaluations and suggestions on possible improvements are then reported to the evaluators, who work on updating the evaluated nuclear data library to a further release. When the real-case simulations designed using the library are in good agreement with

the experimental results, the library is ready for end use and the improvement iterative process for that version of the library is over. Of course, this process refers to nuclear data — such as cross sections, decay constants, fission yields, neutron multiplicity, ... —, but also to their uncertainties, which are of key importance to allow for adequate comparison with the experimental results of the simulated real cases.

As mentioned in section 1.3, this work contributes to *Benchmarking* node of Fig. 2.4, reporting the comparison of the results of three real-case simulations both against experimental results and against each other, when different evaluated nuclear data libraries were used. This thesis also contributes to the connection of nodes *Library* and *Experiments* in Fig. 2.4 in the uncertainty quantification process and library comparison. This kind of analysis allows the evaluators to identify potential weaknesses and missing data in the nuclear data library version and therefore to prioritise new improvements and measurements. The nuclear data libraries used in the reported work are:

- ENDF/B-VII.1 [41]
- ENDF/B-VIII.0 [4]
- JEFF-3.1.2 [5]
- JEFF-3.3 [42]
- JEFF-4.0t1 [7]
- JENDL-4.0u [6]

The data from ENDF/B-VII.1, ENDF/B-VIII.0, JEFF-3.1.2 and the ones from JEFF-3.3 were used as inputs for the reference model calculations of Calvert Cliffs MKP109-P. This is as the comparison of the most recent evaluation with previous ones could be indicative of the library evolution. For the same reason, JEFF-3.3 and JEFF-4.0t1 were used with ENDF/B-VIII.0for the nuclear data uncertainty propagation through the model of Gösgen GU3. For the nuclear data uncertainty propagation in Calvert Cliffs MKP109-P and Takahama SF95-4, ENDF/B-VIII.0, JEFF-3.3 and JENDL-4.0u were used instead.

Some general considerations can be mentioned on the comparison of these nuclear data libraries. ENDF/B-VIII.0 is evaluated to be conservative in terms of uncertainty with respect to the others, which is found also in the reported results. Thanks to the implementation of physical models that complement the experimental results, JEFF-3.3reports more fission product cross section covariance data than ENDF/B-VIII.0, while JENDL-4.0u reports none. JEFF-4.0t1reports more covariance evaluations than JEFF-3.3. On the other hand, more covariance evaluations are given for the actinides' cross sections in JENDL-4.0u than in ENDF/B-VIII.0 and JEFF-3.3, which gives the less of them.

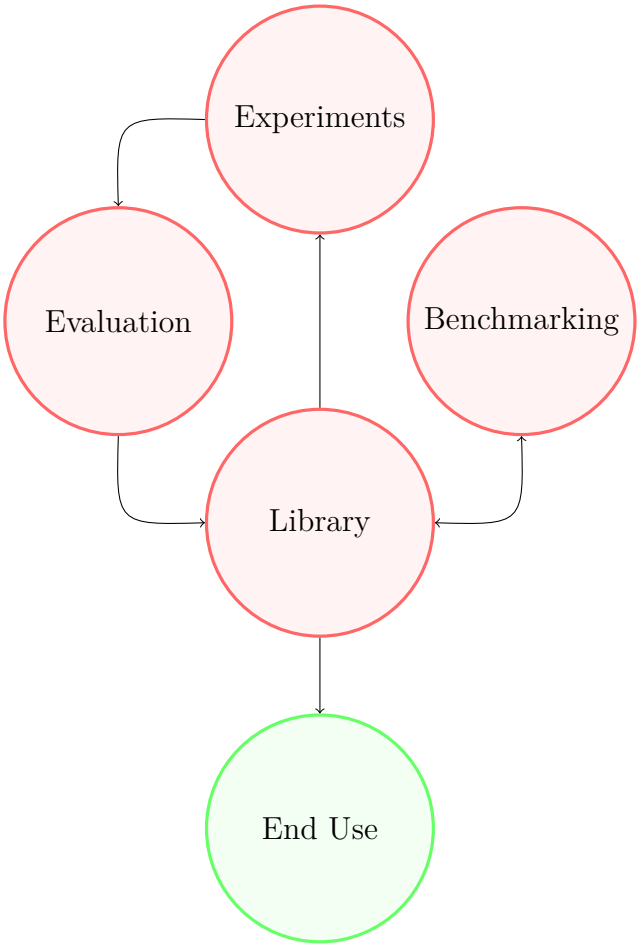

Figure 2.4: Evaluation process scheme.

2.6 Tools

In the following, the main tools and codes used or developed to obtain the reported results are presented. This selected list is representative of the different fields embraced by this thesis work, even though it is not completely exhaustive for the sake of conciseness.

2.6.1 ALEPH-2.8

ALEPH [43] is the MC burnup code developed at SCK CEN since 2004. It couples MCNP or MCNPX [44] to numerical deterministic depletion algorithms, according to what described in section 2.1.4. It guarantees full consistency between the nuclear data used in the depletion calculation and the one used to simulate the

transport as a main feature.

ALEPH has been continuously improved and validated taking into high consideration the user's feedback. In this thesis, ALEPH was used to design one of the models of Gösgen Ariane GU3 to compare to the experimental values. Such a validation was complemented by the comparison with the results of other members of the OECD NEA subgroup 10 [45], which subject is the modelling of that sample. As a matter of fact, ALEPH allows for the design of single-pin models up to full-core simulations, and automatically computes many observables with larger precision when compared to other burnup codes. This makes ALEPH very attractive for SNF calculations.

2.6.2 Serpent-2.1.32

Serpent [46] is a code for three-dimensional continuous-energy MC transport simulation and burnup calculation. It is designed for lattice applications, which makes it specifically oriented towards reactor modelling applications. The burnup calculation capability allows Serpent to independently simulate fuel depletion. When compared to ALEPH, Serpent proves to be much faster for the applications considered[1], for which reason it was used for the many calculations needed in the uncertainty propagation procedure.

Serpent can be used for various reactor physics calculations at pin, assembly and core levels. It also allows for detailed geometrical description in the form of divisions of the pins — e.g. radial division of each pin —, which was used in the design of the models developed in the course of this thesis.

2.6.3 SANDY-0.0.9

The SANDY computer code [8] is a tool for statistical sampling-based uncertainty quantification programmed in Python [47], compatible with Python since version 3.6. Thanks to its API that allows for easy interaction of the user with the nuclear data libraries. SANDY also allows one to process the data stored in ENDF6 format [48] and to generate correlated samples of the nuclear data according to their evaluated best estimate and covariance matrices.

More in the details, the ENDF6 files are read by SANDY from their online source and then processed separately in modules storing their best estimate values and in modules storing their covariance information. These modules allow the user to process and sample the nuclear data, which are then re-written in ENDF6 formatted

[1]Serpent uses the RAM to store the nuclear data. This allows for faster processing of the particle interactions during the MC simulation, but it comes at the cost of larger hardware requirements.

files. SANDY is code-agnostic, in the sense that it allows to process the data from ENDF6 to ENDF6 format. Yet, SANDY also works as a wrapper for NJOY [49], which enables the option to directly process the ENDF6 files to *ace* files. The *ace* files are used by many MC codes even being not valid for all transport codes (MC and deterministic ones).

The correlated multivariate normal distribution sampling procedure implemented in SANDY happens in four steps, following what described in [50]:

1. Normally distributed sets of random samples are extracted using NumPy [51];
2. Cholesky[2] decomposition of the relative covariance matrix C is computed to be $C = L \cdot L^T$;
3. The product of the lower-triangular decomposed covariance matrix L by the normally distributed sets results in correlated sets of random distributed perturbation coefficients;
4. The perturbation coefficients are then multiplied by the best estimate value of the corresponding nuclear datum.

A contribution to SANDY development was also part of this thesis work. This happened mainly in the renewal of the sampling procedure and more in general of the 'cov.py' module. This was possible thanks to GitHub [52], where SANDY source code is available.

The normal distribution is the distribution at maximum entropy, and is therefore a conservative guess when only the best estimate and the standard deviation or covariance matrix of a distribution are provided. This is often the case for nuclear data. The usual choice of multivariate normal distribution sampling is also well justified by the CLT, according to which, when manipulated, the distributions tend to converge to the normal one. Still, negative samples can be computed when sampling a normal distribution. This can lead to non-physical values for many nuclear data such as the cross sections, the decay constants, the fission yields, etc... Moreover, the choice of a distribution is one of the modelling assumptions, as discussed in section 2.3.

One might then want to assess the bias given by this assumption considering different distributions for the sampling procedure. This kind of analysis is out of the scope of this work, yet a contribution to the implementation of the sampling according to the lognormal and to the uniform distribution was part of the effort

[2]In practice, evaluated covariance matrices often have out-of-bounds correlations — i.e. $\rho < -1$ or $\rho > 1$ — or determinant 0. This makes the Cholesky factorisation impossible, therefore alternative decompositions shall be used. The so-called QR decomposition is implemented in SANDY as R^T converges to L when the conditions for Cholesky decomposition hold.

of this thesis work. This was done in collaboration with Enrica Belfiore, who will present this topic with more detail in her master's thesis [53].

In this work, SANDY was used to process the results of ALEPH and to perform the statistical sampling procedure of the cross sections, as described in section 2.4.

2.6.4 JANIS

JANIS [54, 55] is a Java-based software designed to allow for easy and user-friendly manipulation of nuclear data. It exists in two versions, a desktop one and an online one. An example of the user interface of the desktop version of JANIS is reported in Fig. 2.5. JANIS was used in the course of this thesis work for the comparison of cross sections and of different evaluations as well as of the evaluated standard deviations. Its simplicity and broad scope make it a handy tool for fast analysis and insight verification. JANIS is therefore the basis for all the physical interpretation of the reported results when it comes to numerical comparison and order of magnitude evaluation. The PWR spectrum weighting function for the energy dependent cross sections implemented in JANIS was often used in the course of this thesis work.

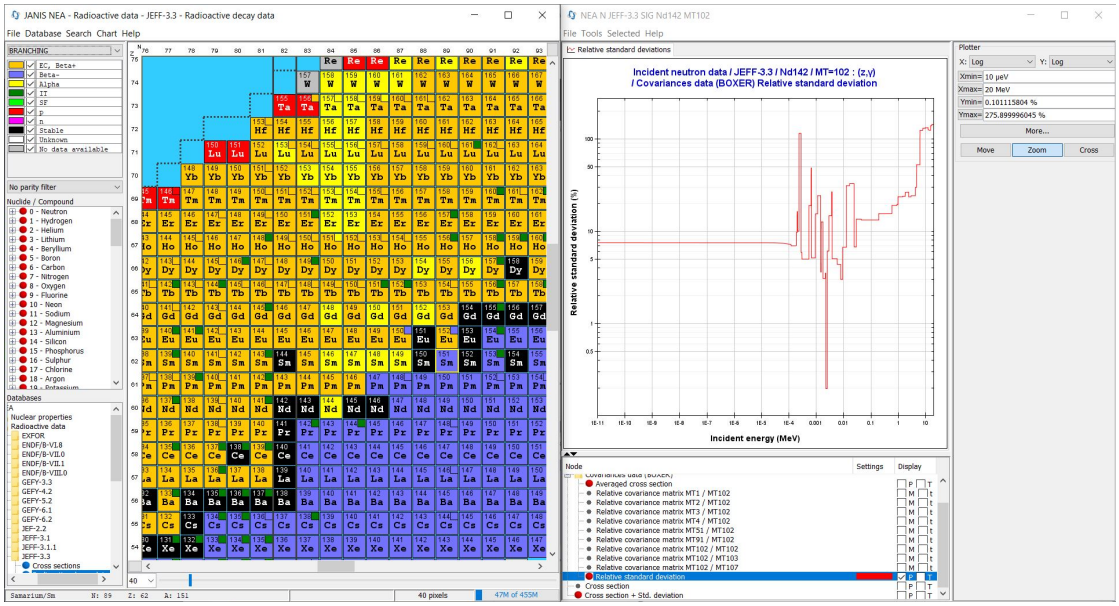

Figure 2.5: JANIS desktop user interface

2.6.5 One-Group cross section data frame

A ‘Pandas‘ [56, 57] DataFrame with the one group cross sections evaluated by ENDF/B-VIII.0, JEFF-3.3, JEFF-4.0t0, JEFF-4.0t1 and JENDL-4.0u was produced. There, the cross sections were averaged over a standard PWR spectrum to have a numerical comparison of the differences in the evaluation. This was done mainly to estimate the changes from JEFF-4.0t0 and JEFF-4.0t1 from JEFF-3.3. The implementation is for the moment limited to the nuclides directly relevant for the SNF(Refs. [20, 21]), but not to their precursors. Also, only the best estimates averaged were compared. Extending such an analysis to the uncertainties and to those precursors would make this tool rather useful in this kind of analysis.

While JANIS allows for qualitative raw uncertainty comparison and uncertainty propagation through MC models is completely tailored on the application, this tool allows for the realistically weighted uncertainty comparison. This would result in relevant preliminary results at a much smaller computational cost when compared to statistical sampling uncertainty propagation and ANOVA.

2.6.6 SFCOMPO-2.0 database

SFCOMPO-2.0 [54] is the publicly available database for experimental assay measurement of OECD NEA. It provides nuclide concentrations measured by radiochemical DA supplemented with fuel design and operational data. SFCOMPO-2.0 enables easy access to the experimental datasets for several reactors and the references relative to the studies.

SFCOMPO together with the benchmark guidelines for the case study samples enabled for detailed model design and comparison with experimental data.

2.7 Spent nuclear fuel composition measurement techniques

Two main manners to analyse SNF samples exist, and those are often practiced one after the other. On the one hand, non-destructive analysis NDA considers the SNF as a whole emitting radiation. These radiations are then measured and considerations on the composition can be derived from this. This kind of analysis is often performed on fuel spent assembly [58]. On the other hand, DA is often applied to SNF samples directly. This often implies sample dissolution in acidic streams and successive composition analysis through component separation.

The separation process efficiency is high, but not complete, which causes part of the uncertainty of the experimental results. To this, sample cutting and weighting, sample dilution, nuclide inventory analysis and calculations, both in terms of processing and similarity coefficients, should be added as uncertainty sources in

the process. Of course, not all nuclide concentrations are affected by the same uncertainties the same way. Namely, concentration of metallic fission products tends to be underestimated in the radio-chemical analysis (examples in Refs. [12, 14]).

Chapter 3

Description of the modeled samples and design of the simulations

3.1 Calvert Cliffs - Sample P

Fuel assembly D047 was irradiated in the Calvert Cliffs PWR unit 1 between 1977 and 1980 for four consecutive cycles — from cycle 2 to cycle 5. The assembly design is a 14×14 assembly with 176 fuel rods and 5 guide tubes by Combustion Engineering [59].

3.1.1 Model description

The assembly D047 was modeled in the Serpent considering design parameters provided by [60] and by SFCOMPO, as reported in[61]. The modeled assembly is reported in Fig. 3.1.

Reflective boundary conditions were imposed on the assembly sides, assuming a flat neutron flux profile as if the assembly D047 was in the center of the reactor. This approximation is usually acceptable as long as the assembly is not taken from the vicinity of the lattice boundaries, as reported in [62, 13]. Single-enrichment-level UO_2 fuel loaded at the beginning of the irradiation was modeled. This was set to 3.038% for all pins in the assembly, according to the benchmark specifications [63]. Values from table 68 in [64] were used for modeling the boron concentration in water. Ref. [65] allowed for the extraction of the modeled assembly power history details. The normalisation of those values for the considered sample result a burnup of 44.13 $\frac{\text{GWd}}{\text{tHM}}$ in sample P at the end of irradiation cycle 5. This value was based on ^{148}Nd measured and computed content and is the same as the one used in Ref. [64]

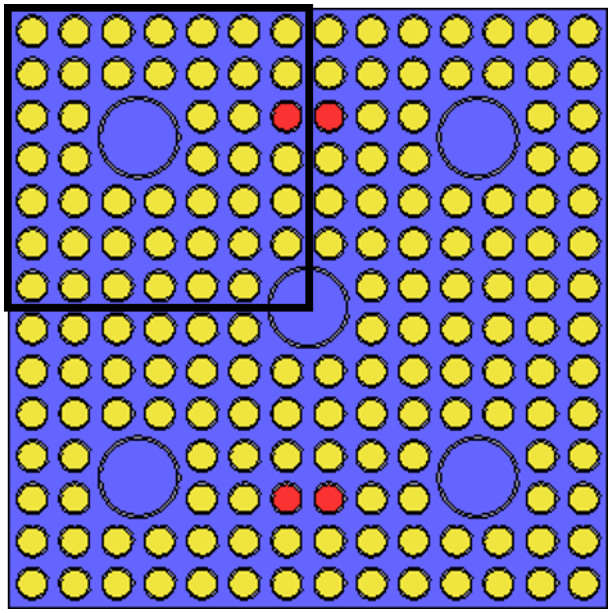

Figure 3.1: Two dimensional lattice of the assembly D047 of Calvert Cliffs.

and was used for SCALE 5 validation. The sample power density and the boron concentration modeled are reported in Fig. 3.2.

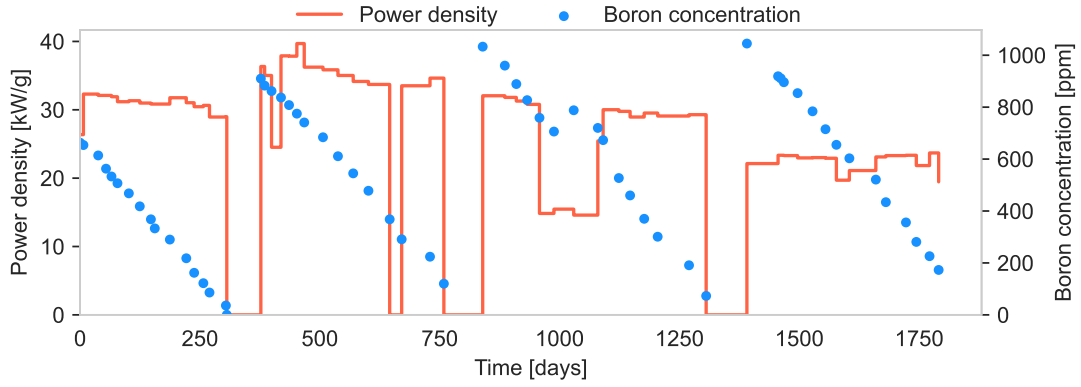

Figure 3.2: Calvert Cliffs MKP109-P: Sample power density and boron concentration considered in Calvert Cliffs sample P model.

Moderator and fuel density and temperature were modeled as constant along the four cycles and their values were computed from [66]. The described model as well as its simplified version was already developed at SCK CEN, where those were developed in the framework of EURAD project (WP8, ST2.1) [2].

The predicted sample inventory at discharge is reported in Appendix B. Four

simulations considering different evaluated nuclear data libraries — ENDF/B-VII.1, ENDF/B-VIII.0, JEFF-3.1.2 and JEFF-3.3, namely — were computed. Overall good agreement in absolute value terms is noticeable there. In the next section, a comparison in terms of discrepancy from the experimental results is presented.

3.1.2 Comparison with experimental results

The SNF characterisation of sample P in rod MKP109 of the described assembly was modeled. The sample was situated at 165.22 cm from the bottom of the fuel. This justifies the choice of designing a bi-dimensional model, as the neutron flux is flatter further from the fuel assembly extremities when considering the vertical direction; the sample P was located close to the assembly mid-plane. Radio-chemical measurement campaigns were performed on this sample at the PNL and at the KRI. There, the concentrations of many actinides and fission products were evaluated at PNL after a decay time of 1870 days and at KRI after a decay time of 5656 days; additional fission products were measured at PNL after a decay time of 3817 days and then adjusted to 1870 days, as reported in [67]. All the mentioned decay times are referred to the decay time after irradiation cycle 5. The results reported in the following were obtained adjusting the measured concentrations to the end of irradiation time, which allows for the comparison of the simulation results with the experimental ones. The nuclide composition of sample MKP109-P was assessed several times in the years as presented in [62].

The comparison of the Serpent model prediction with the experimental results is reported in the form of C/E-1 in Fig. 3.3. The comparison is here reported for the set of nuclides which measured values and uncertainties are given in SFCOMPO. This is limited when compared to the one measured in the experimental campaign conducted on this sample and its later updates. A comparison over a broader set is reported in [61]. The experimental uncertainty is reported in Fig. 3.3 in the form of error bars representing the range of one standard deviation from the experimental best estimate value. Some outliers with discrepancies larger than 30% were found, namely ^{149}Sm, ^{151}Eu, ^{152}Eu, ^{154}Gd, ^{156}Gd, ^{157}Gd and ^{158}Gd and are not reported in Fig. 3.3. Despite this, many results are within the range of one standard deviation from the experimental measured ones and almost all of them are in the range of two standard deviations. The model predictions are also in line with the results reported in [67, 40]. Often, the results obtained with the different nuclear data libraries follow a similar trend in terms of over- or under-estimation of nuclide inventory in the sample after irradiation.

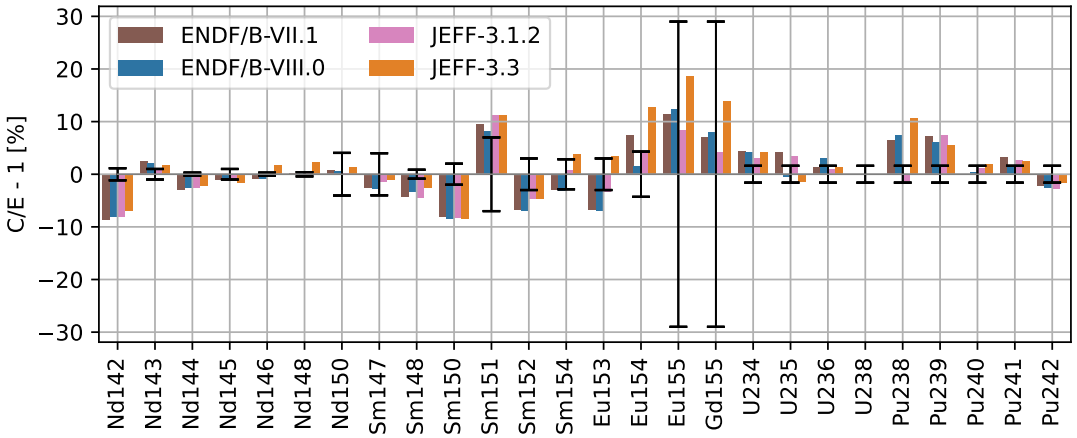

Figure 3.3: Calvert Cliffs MKP109-P: Deviation (in percent) between calculated (C) and experimentally measured (E) concentrations as C/E-1. The error bar represents the experimental error as one standard deviation.

3.1.3 Model simplifications

To perform statistical sampling, the same model is run several times with perturbed input parameters. Doing this with the model described in section 3.1.1 would require excessive computational time, as discussed in [25, 22, 68]. For this reason, some simplifications were included in the model to reduce its computational cost enabling multiple simulations to run in parallel. These simplifications come at the cost of a bias in the model, which will be less representative of Calvert Cliffs assembly D047 irradiation history, resulting in less accurate sample composition results. The possibility to consider the uncertainty results obtained from the statistical sampling performed on the simplified model applicable to the concentrations computed in the accurate one is not analysed in detail. On the other hand, this procedure allows for order of magnitude evaluation, still relevant in uncertainty studies, and also allows for a certain degree of generalisation. In other words, looking for similarities among LWRs in terms of uncertainty propagation and sensitivities is one of the underlying topics of this thesis (for which future work complement is of course needed); in this sense, being specifically representative of Calvert Cliffs is not as relevant as being representative of a PWR-like reactor.

This is obtained in the simplified model described in the following. The simplifications to the model are:

- the number of particle histories tracked per transport simulation was reduced by a factor 10;
- no predictor corrector scheme was included in the simulation;

- average cycle boron concentration was modelled;
- only three depletion zones were considered:
  1. the fuel sample;
  2. the fuel rods adjacent to the sample;
  3. the remaining fuel rods.

The effect of these simplifications was assessed through concentration results comparison, reported as C/C-1 (simplified over accurate) in Fig. 3.4. For this comparison, best estimate nuclear data from ENDF/B-VII.1 were used for both models. Among the discrepancies introduced by the simplifications highlighted in

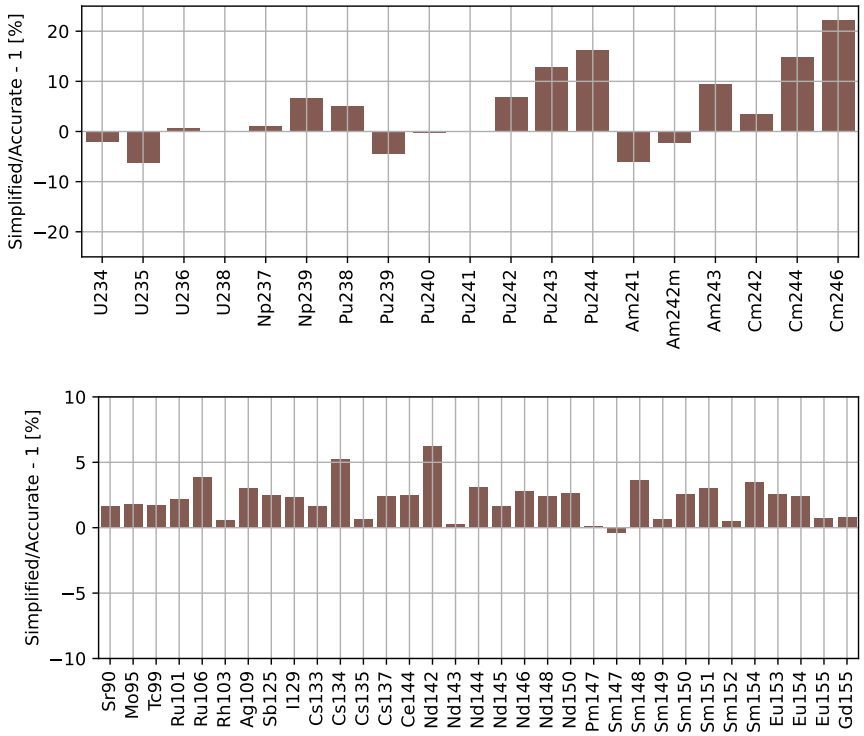

Figure 3.4: Calvert Cliffs MKP109-P: Deviations (in percent) on nuclide concentrations (also called C/C-1) introduced by model simplifications. The ratio denominators are the results of the accurate model. Calculations were run in both cases with ENDF/B-VII.1.

Fig. 3.4, the difference in ^{148}Nd is of major relevance as it indicates an overestimation of the sample burnup of about 2%, corresponding to larger irradiation in the simplified model. This effect is also reflected in the lower concentration of ^{235}U

computed with the simplified model. The burnup overestimation, also results in the larger production of fission products and of further actinides, respectively due to the more fissions and transmutations taking place in the sample.

A non-complete interpretation and explanation of such discrepancy is reported in Appendix A.

3.2 Gösgen - Sample GU3

Assemblies FA 16-01 and FA 17-01 were irradiated in the Gösgen PWR reactor. Both are 15×15 assemblies with 20 guide tubes and fueled with UO_2. The GU3 fuel sample was irradiated for two cycles — cycle 16 and cycle 17 — in FA 16-01 and for one cycle — cycle 18 — in FA 17-01.

The initial fuel enrichment of the fuel in assembly FA 16-01 was 4.1% in ^{235}U, while for cycle 18 the GU3 sample was inserted in a previously irradiated fuel assembly, whose burnup was considered to be approximately 20 $\frac{\text{GWd}}{\text{tHM}}$.

It is also worth mentioning some rod shuffling happened in the fuel assemblies where the GU3 sample was irradiated. The GU3 sample irradiation was modelled in Serpent according to the benchmark specifications given in [69].

3.2.1 Description of the models

The GU3 sample was modelled both in ALEPH and in Serpent. As mentioned, this was done neglecting the rods shuffling and setting up a different simulation for each cycle. There the fuel compositions given in the benchmark were implemented for cycle 16 and for cycle 18, while the output material composition of cycle 16 was used as input for cycle 17. The fuel sample composition at beginning of cycle 18 was taken from the results of the calculations for cycle 17. Each cycle was modelled to have a time dependent power history. This was normalised to ^{148}Nd experimental concentration resulting in a sample burnup of 52.5 $\frac{\text{GWd}}{\text{tHM}}$ at the end of cycle 18, rather coherent with what is given in the benchmark, 52.504 $\frac{\text{GWd}}{\text{tHM}}$. Constant material densities, temperatures and constant boron concentrations were modelled for each cycle according to the benchmark. The considered temperatures were 1200 K, 1000 K and 900 K for the fuel in three three modelled cycles and 600 K in the cladding and in the moderator during each cycle. The sample power density evolution in the three cycles as well as the boron concentration in water is reported in Fig. 3.5.

All the three simulations described the assembly in four regions: two for the two most external rings of pins, along the fuel assembly perimeter, one for the rods adjacent to the sample and one for the sample itself. For these calculations, ENDF/B-VII.1 nuclear data library was used. The ALEPH version of this model was developed in a thesis work performed at SCK CEN [70]. That model was made

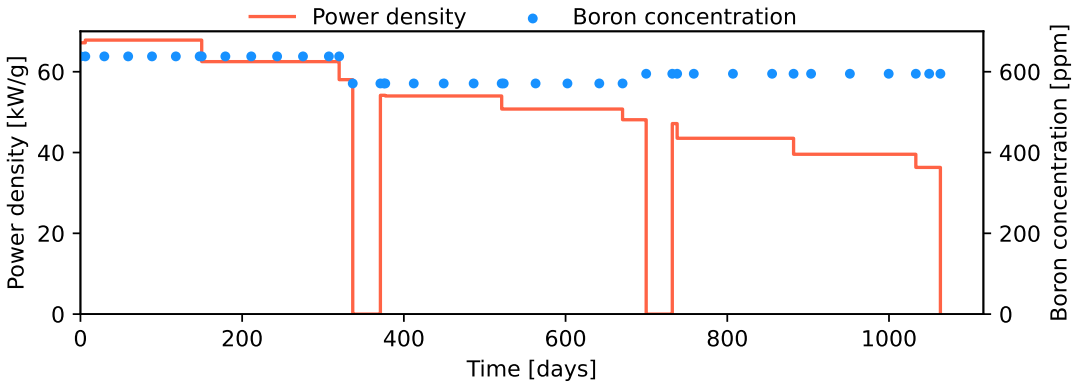

Figure 3.5: Gösgen GU3: Sample power density and boron concentration.

compliant with the benchmark specifications and commuted to Serpent to enable the uncertainty propagation procedure. Reflective boundary conditions were considered for both models. This is compliant with the benchmark specifications and a good approximation given the vicinity of the sample to the assembly mid-plane.

The sample inventory predicted at discharge is reported in Appendix B.

3.2.2 Comparison with experimental results

The nuclide composition of the modelled GU3 sample was assessed trough an experimental campaign carried out at SCK CEN and ˙ITÜ laboratories.

The results computed with the ALEPH model were then compared to those experimental results. Such comparison is reported as C/E-1 in Fig. 3.6. There, pretty good agreement of the computed concentrations with the experimental ones is visible: many nuclides present calculated concentrations in the range of one standard deviation from the experimentally measured concentrations and only a number of discrepancies exceeds the two standard deviations. The differences are due to the limited detail of the model, where some relevant assumptions were included and bias is therefore visible in Fig. 3.6. Only ^{234}U presents a discrepancy larger than 30%, and was therefore excluded from the plot.

The concentrations and the value of k_∞ estimated at each irradiation step were also compared with the results of other participants and institutions taking part in the benchmark. This comparison proved good agreement of the presented model results to the others designed following the same benchmark [69]. During the meeting in which the results were discussed, considering the large over-prediction of ^{234}U given by the many codes and library used by the participants, a possible error in the estimation of the sample initial ^{234}U was proposed. Moreover, the possibility of a measurement error on the concentration of ^{103}Rh was mentioned.

These assertions will of course need to be further investigated before moving to the next steps of the subgroup work.

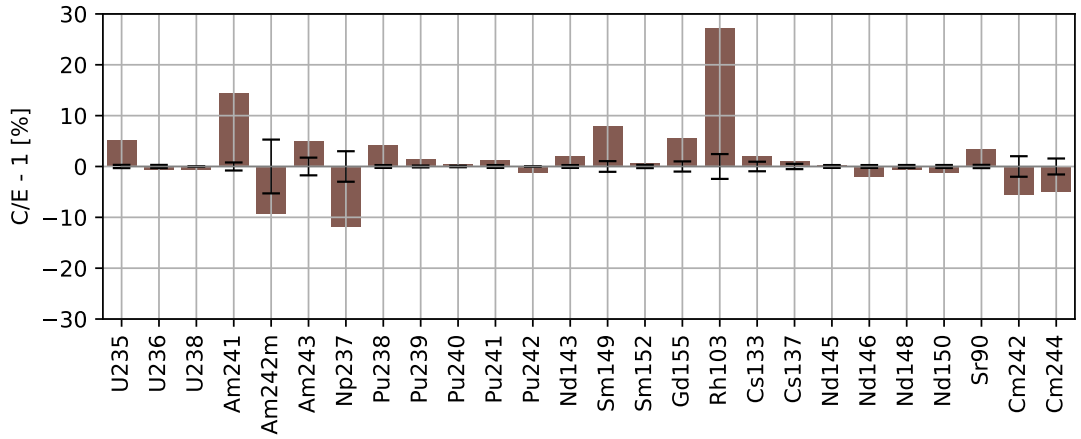

Figure 3.6: Gösgen GU3: Deviation (in percent) between calculated (C) and experimentally measured (E) concentrations as C/E-1. The error bar reports the experimental error as one standard deviation.

3.2.3 Model simplifications

As discussed in section 3.1.3 for the case of Calvert cliffs, some model simplifications are needed to reduce its running time, smoothing the statistical sampling procedure. To do so, given the much smaller running time of Serpent, the ALEPH model was reproduced in Serpent. Some slight differences due to the inherent differences among the two codes are unavoidable. Moreover, a better spatial discretisation was considered in the Serpent model. There, each fuel pin — including the fuel sample — was divided in 10 annular sub-regions, while on the other hand the same assumptions on the time-varying parameters and on the materials as in ALEPH model were considered. The Serpent model concentration results were then compared to the ALEPH ones in the form of C/C-1. Such comparison is reported in Fig. 3.7.

Fig. 3.7 highlights the effect of the main changes from the ALEPH model to the Serpent one. The comparison is reported for the same set of nuclides used for the ALEPH model validation against experiments. Overall very good agreement among the two models is found.

The 10 radial divisions considered in the Serpent model allow to better describe the in-pellet power distribution as well as the RIM effect and the breeding of plutonium isotopes. The larger amount of ^{239}Pu bred at the pellet surface makes

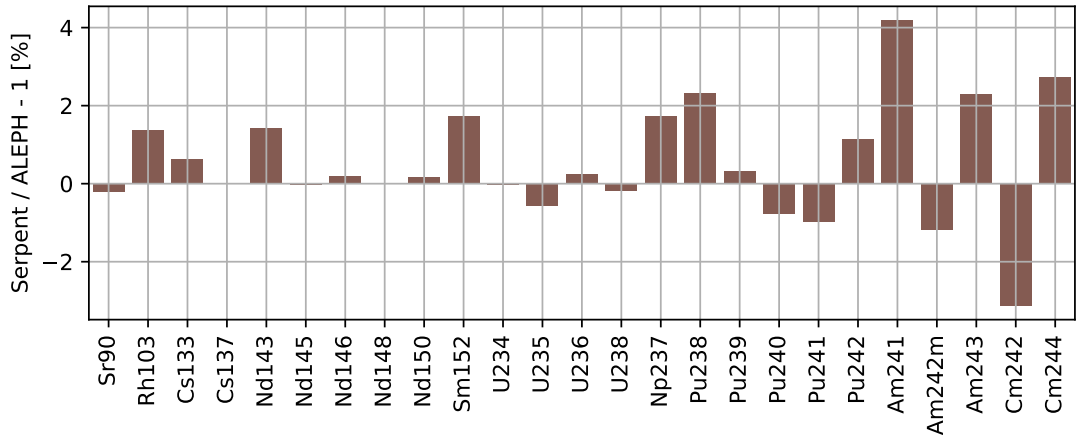

Figure 3.7: Gösgen GU3: Deviations (in percent) on nuclide concentrations (also called C/C-1) introduced by model reproduction. The ratio denominators are the results of the ALEPH model. Calculations were run in both cases with ENDF/B-VII.1.

its concentration slightly increase in Serpent. This is reflected by the decrease in concentration of ^{239}Pu reported in Fig. 3.7. As a consequence, and because of the correlation between fissionable isotopes introduced by the power normalisation constraints, the predicted concentration in ^{235}U is smaller with Serpent. The same holds for ^{241}Pu, which is more easily produced by neutron captures in lower-mass-number plutonium isotopes but is also fissionable, resulting in a lower concentration.

Good agreement is also found for the fission product concentration prediction. The fluctuations there are both related to the different fission yield of the fissioning nuclides (more ^{235}U fissions in the Serpent model), to the statistical error, and to the other slight differences in the models.

The same simplifications described in section 3.1.3 were then introduced in the Serpent model for GU3. This simplification resulted in a bias which effect is reported in Fig. 3.8, for the set of nuclides on which the uncertainty was propagated.

Considering the simplifications needed to reduce the running time of this more complex model, the reported agreement is satisfactory being almost always in the range of 10%. The discrepancy in the concentration of ^{148}Nd indicates a non-matching of the burnup in the simplified model. The reasons of this are further investigated in Appendix A.

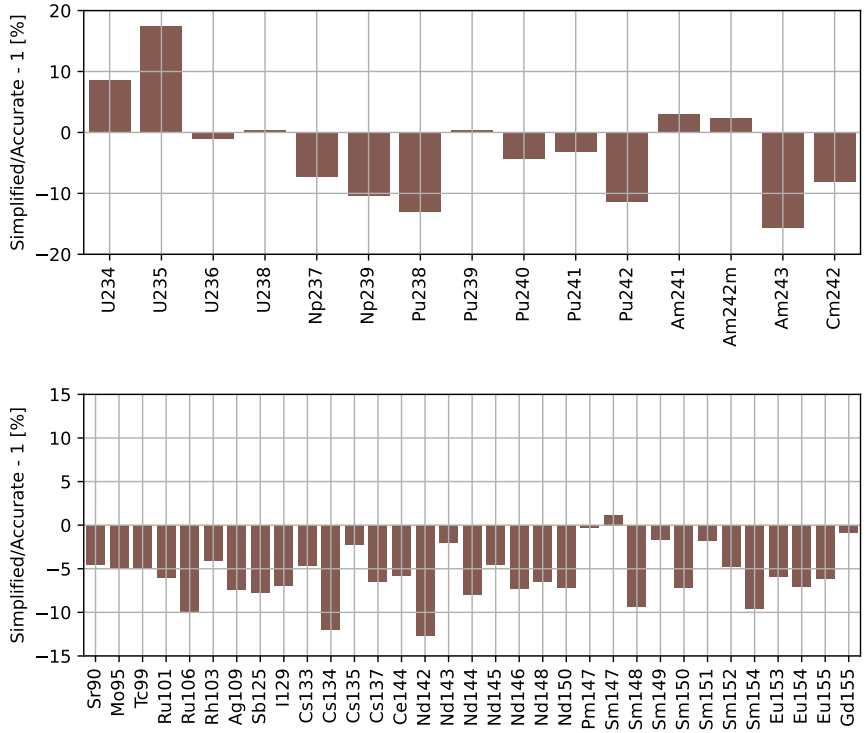

Figure 3.8: Gösgen GU3: Deviations (in percent) on nuclide concentrations (also called C/C-1) introduced by the Serpent model simplifications. The ratio denominators are the results of the accurate model. Calculations were run in both cases with ENDF/B-VII.1.

3.3 Takahama - Sample SF94-5

Takahama SF95-4 sample was irradiated in Takahama unit 3 PWR for two cycles. Assembly NT3G23, where the sample was located, is a 17 × 17 fuel assembly and the initial enrichment of the sample was 4.1 wt.% in ^{235}U. Of the 289 rods in the fuel assembly, 24 were guide tubes, 1 used to host in core instrumentation and the others were made of UO_2 fuel. Of the 264 fuel rods, 16 also used to be enriched with gadolinium.

3.3.1 Model description

The assembly NT3G23 was modelled in Serpent according to the specifications given in SFCOMPO-2.0 database and in Ref. [71]. The modelled assembly is shown in Fig. 3.9. Reflective boundary conditions were adopted for this model, which is often an acceptable approximation as long as the fuel assembly is not taken from

the lattice boundaries, as discussed in section 3.1.1. The material temperatures were taken from [72]. The flux was normalised to the sample burnup of 36.69 $\frac{\text{GWd}}{\text{tHM}}$, which was estimated based on the measured ^{148}Nd concentration [72]. All the fuel rods were modelled to have the same initial enrichment of the sample. The sample power history and boron concentration taken from SFCOMPO are reported in Fig. 3.10. No predictor-corrector scheme was implemented in this model. The described model, as well as its simplified version, were already developed at SCK CEN in the framework of EURAD project (WP8, ST2.1) [2].

The so-predicted discharge sample inventory, computed using nuclear data from ENDF/B-VII.1, is reported in Appendix B.

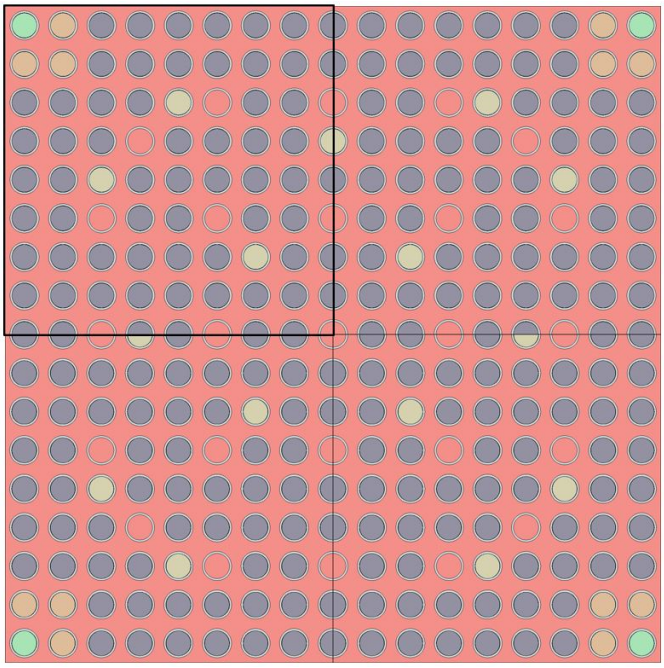

Figure 3.9: Two dimensional lattice of the assembly NT3G23 of Takahama.

3.3.2 Comparison with experimental results

The experimental campaign on the Takahama SF95-4 sample was performed at JAERI. The results of those experimental assessments were reported to the sample discharge date [60]. The estimated experimental uncertainties range from few decimal points for the concentration of uranium isotopes, up to 10% for the concentrations of minor actinides and of some fission products, respectively measured through α and γ spectroscopy.

The comparison with experimental results gives overall quite good agreement,

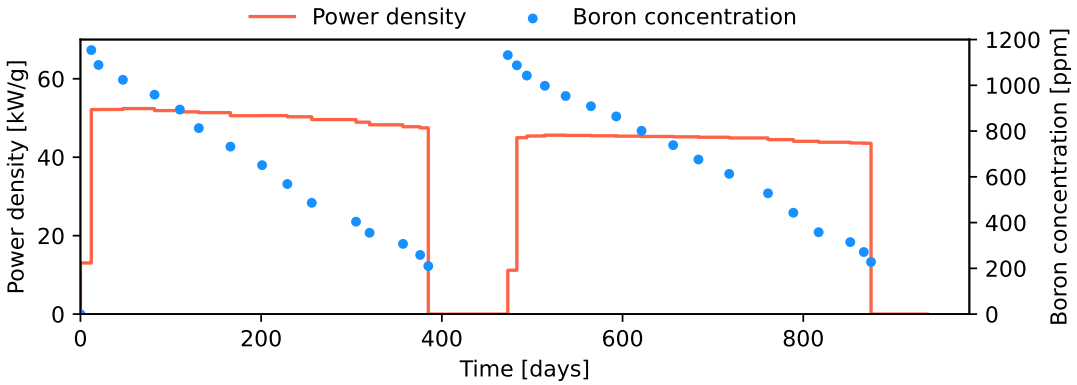

Figure 3.10: Takahama SF95-4: Sample power density and boron concentration considered in Takahama SF95-4 model.

with discrepancies often below or in the range of 10%. The experimental uncertainty is reported in Fig. 3.11 in the form of error bars. A number of outliers was excluded from the plot, being its discrepancy larger than 30%, namely ^{241}Am, ^{242}Cm, ^{106}Ru and ^{125}Sb. The disagreement in the plutonium isotopes might be originating from the vicinity of the sample to the assembly boundaries, which makes its concentration results more affected by the assumption of reflective boundary conditions. The results of such a comparison with the data measured at the Japanese national laboratory are reported in Fig. 3.11.

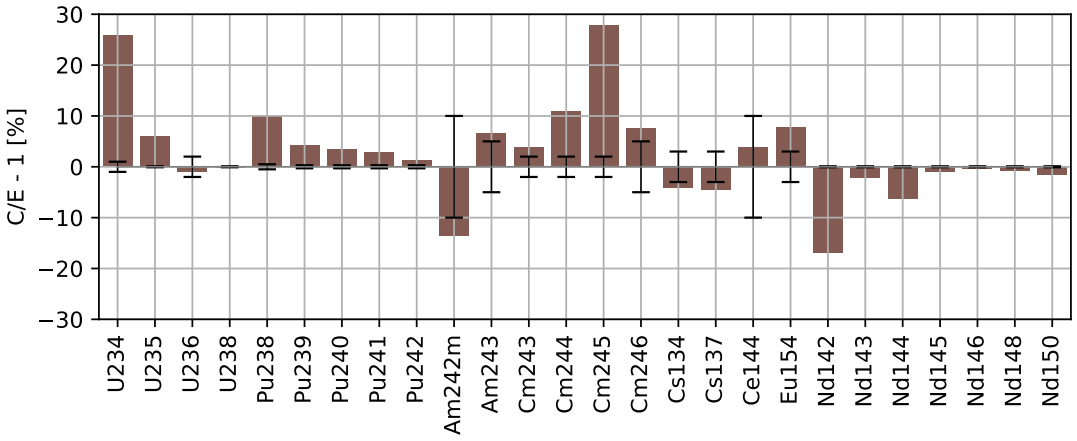

Figure 3.11: Takahama SF95-4: Deviation (in percent) between calculated (C) and experimentally measured (E) concentrations as C/E-1. The error bar represents the experimental error as one standard deviation.

3.3.3 Model simplifications

The same model simplifications as the ones introduced in the previously described models were considered for the model of Takahama SF95-4. A very good matching of the results of the two simulations was found and is reported in Fig. 3.12. There, discrepancies lower than 10% and in many cases lower than 5% are displayed, when the set of nuclides used for the uncertainty propagation is considered.

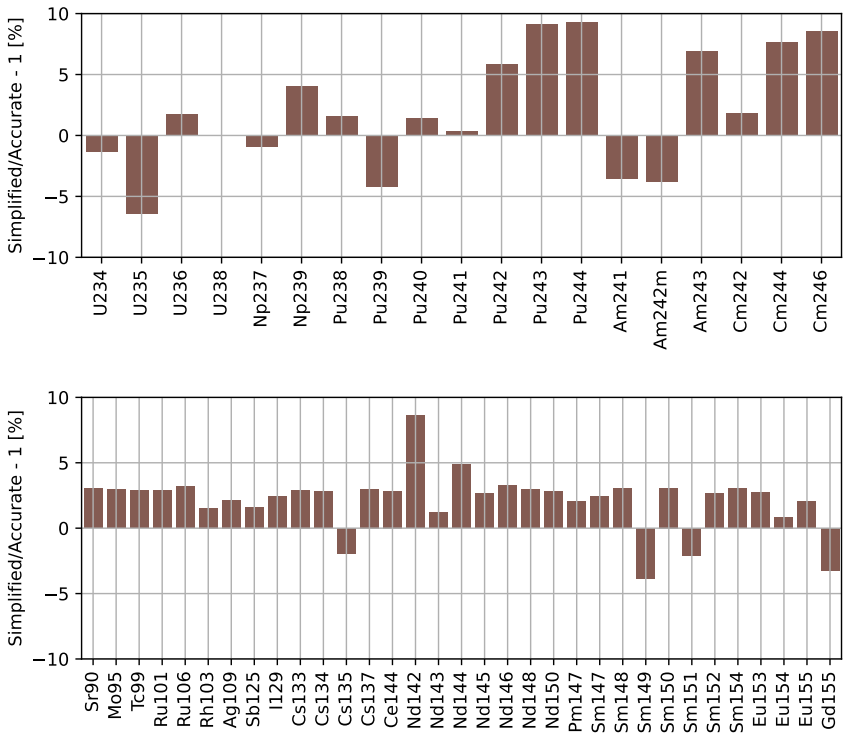

Figure 3.12: Takahama SF95-4: Deviations (in percent) on nuclide concentrations (also called C/C-1) introduced by the Serpent model simplifications. The ratio denominators are the results of the accurate model. Calculations were run in both cases with ENDF/B-VII.1.

Chapter 4

Sensitivity analysis and uncertainty propagation

4.1 Calvert Cliffs MKP109-P

Uncertainty was propagated through the Serpent simplified model of Calvert Cliffs described in section 3.1.3. To do so, the SANDY code was used to statistically sample the perturbation coefficients, to be multiplied by the best estimate evaluated cross sections in the considered nuclear data libraries, namely ENDF/B-VIII.0, JEFF-3.3 and JENDL-4.0u. The perturbation coefficients were sampled according to multivariate normal distributions, with mean 1 and covariance matrix given in the considered nuclear data libraries. This was done following the procedure described in section 2.6.3. Uncertainties on other nuclear data types (such as fission yields, fission neutron multiplicities, energy/angular distributions, etc.) were not propagated. Ref. [25, 73] further investigate the effect of this assumption, proving it to be neglecting minor contributions to the total output uncertainty — such as the one deriving from decay data — or highlighting the need of a more detailed discussion on some of the not considered uncertainty sources, for which no covariance matrix is provided — such as the fission yields.

For each of the three nuclear data libraries considered, 200 sets of sampled perturbation coefficients were taken for the cross sections of the actinides and 100 sets were taken for the cross sections of the fission products. This choice was guided by the considerations on Fig. 2.1, reported in section 2.3. Each of these sets was processed with NJOY[49] code and was replaced in the respective nuclear data library. This resulted in an model input data-set consisting of data from ENDF/B-VII.1 for the majority of the nuclear data and from the perturbed nuclear data library for the cross sections. Even if not fully consistent, this procedure is rather effective in the uncertainty propagation as one can expect the sensitivity

of the model output to the inputs to be basically unchanged even considering the different evaluations for the other nuclear data. The cross section perturbed data were produced at 900 K. This was to reduce the computational burden of repeating the sampling several times. The effect of this assumption on the SNF observables is reported in [74]. Moreover, the possible bias introduced by the different temperature of the sampled cross sections is further attenuated by the on-the-fly resonance broadening [75] implemented in Serpent: with proper simplifications, Serpent can automatically adjust the cross section value to the fuel temperature during the simulation.

For the actinides, all the three evaluated nuclear data libraries provide covariance matrices. All the available covariance matrices for uranium, neptunium, plutonium, americium and curium isotopes were sampled. Only ^{241}Am covariance given in JEFF-3.3 was not processed as it would require a dedicated procedure. For fission products, only the cross sections of nuclides with atomic number between 33 and 65 were perturbed. This was done only for ENDF/B-VIII.0 and JEFF-3.3, as JENDL-4.0u does not provide any covariance matrix for the considered fission products. The processing of the covariance matrix of ^{103}Rh presented an error a posteriori, resulting in the non-propagation of its cross section uncertainty.

The contribution to the model output total uncertainty given by the statistical error inherent to MC was also assessed. This was done running 100 simulations with different seed. Hence, the total output uncertainty was computed to be as in Eq. (4.1) for each i-th component of the array of nuclides of the sample after irradiation. Eq. (4.1) accounts for both the nuclear data uncertainty $u_{i,ND}$ and the statistical error $u_{i,STAT}$ in the evaluation of the total concentration uncertainty u_i. This is computed under the assumption of equal statistical error in all the different simulation runs due to the counting statistics and assuming no correlation among fission products and actinides variances, as those were propagated independently. Eq. (4.1) also implies model linearity, according to what discussed in [39].

$$u_i^2 = u_{i,ND}^2 + u_{i,STAT}^2 \qquad \forall\ i \text{ in considered nuclides} \tag{4.1}$$

Before moving to the more detailed analysis of the uncertainty propagation results on actinides and fission product concentrations, it is worth recalling three concepts of major importance for their interpretation. When performing such an analysis, one should bear in mind that each nuclide concentration is affected by the nuclear data of that nuclide, but also by the nuclear data of its precursors. This means that the uncertainty propagates to the analysed nuclide from each of the nuclides that contribute to its production (and removal). Neglecting higher order effects, such as the effect each nuclide has on the neutron spectrum, which then affects the concentration of the analysed nuclide, allows one to consider this effect basically related to production through neutron capture or fission and to decay, which often is β-decay in this context. Considering the uncertainty of decay data and of

fission yields was not propagated, this basically reduces the effect of uncertainty propagation through production paths to neutron capture cross section uncertainty propagation to a certain nuclide from all those nuclides contributing to its formation either by capture or decay. Examples of this will be given in the following. It is also to be mentioned that this is just an insight coming from physical considerations that can help interpret some results, but it does not guarantee complete interpretation as each of the production processes should be weighted on its probability to happen, which is tightly bounded to the neutron flux (comparison of reaction rates and decay constants can help in this). This analysis could be performed through ANOVA which is out of the scope of this work given the larger amount of samples that would be required to perform such an analysis.

One should also bear in mind that not all covariance matrices are given in the considered nuclear data libraries and that few of them were not considered even if given due to processing issues. This lack of data will reflect on the uncertainty propagation results: the missing covariance evaluation of the cross sections of some nuclides results in the impossibility to propagate the uncertainty for those data, which is the same as considering no uncertainty on those. This results in an underestimation of the uncertainty. This effect will of course combine with the production paths uncertainty propagation just discussed. For this reason, one should keep in mind that lower uncertainty in the concentration resulting from calculations with different nuclear data libraries does not necessarily mean one evaluation is better that the other, as some relevant covariance matrices might be not included in that evaluation.

A most clear example of this is the fission product concentration uncertainty obtained using JENDL-4.0u. There, the impossibility to propagate uncertainty due to the lack of covariance matrices virtually results in no uncertainty on fission product concentration, which is just the result of neglecting all the uncertainties[1].

Finally, one should consider that the most relevant uncertainties are in the neutron capture cross section, which is representative of the most relevant neutron-induced removal phenomenon. For this reason, in the following, some uncertainties will be related to the neutron capture cross section uncertainty, which will at least partially justify them. Of course this discussion is even of major relevance for the fission products, whose fission probability can be neglected.

Overall, the uncertainty of the available cross section covariance evaluations gave smaller uncertainty predictions for the fission products' concentrations than for the actinides' one. This is likely to be related to the larger number of nuclides involved in the production of many fission products (via decay and neutron captures), which

[1]This refers to the uncertainty propagation procedure where fission product cross sections were perturbed. The contribution of actinides is of course included in the propagation using JENDL-4.0u, even if it is of minor importance as discussed in section 4.1.2.

reduces the relevance of the larger uncertainties while makes it more likely to have lacks of covariance evaluation along the production path. Apart from few outliers, uncertainties below 5% were predicted for the concentration of fission products. Here it is recalled that the uncertainty was propagated only from the cross section, neglecting other uncertainty sources such as the fission yields, which inclusion would affect such small uncertainty results.

The results presented in the following three sections were also presented in [61], the JEFF nuclear data week in April 2022 [76] and at the PHYSOR2022 conference [61].

4.1.1 Actinides

The effect of nuclear data uncertainty propagated to the actinides' concentration uncertainty in the array of Calvert Cliffs MKP109-P is reported in Fig. 4.1. The results are reported to the time when the measurements were performed or at the time of KRI measurements for the non-measured nuclides. The uncertainties refer to the same time considered when computing the C/E-1 calculation (section 3.1.2), namely sample at end of irradiation. The uncertainty inherent to the MC method, even increased by the model simplifications, among which is the reduction of neutron histories, is assessed to be negligible with respect to the uncertainty propagated from the cross sections. Also the contribution of fission product cross section uncertainty resulted to be negligible, with peaks of the order of 3%. This is coherent with the phenomenological interpretation presented, as the cross sections of fission products (and their concentrations) will influence the neutron flux which then affects the transmutations of the actinides, resulting in an effect on their concentrations which would be not direct.

The uncertainty difference in the concentration of ^{235}U among the results computed using the three different libraries is reflective of the different uncertainty evaluations provided by each library. This results in an uncertainty of the order of 2% when JEFF-3.3 and JENDL-4.0u are considered, and in an uncertainty exceeding 5% when ENDF/B-VIII.0 data are used. Since the production of ^{235}U is much less relevant than its consumption either by neutron capture or by neutron induced fission, the relevance of these reactions is much higher than any other. For the same reason, ^{235}U is expected to be the main — rather only — contributor to its concentration uncertainty in this analysis. Similar considerations hold for ^{236}U. The behaviour of its concentration uncertainty reported in Fig. 4.1 is justified by ^{236}U production path, which main route is neutron capture in ^{235}U: ^{235}U(n, γ)^{236}U. No change in the uncertainty propagated using JEFF-3.3 data is visible from ^{235}U to ^{236}U. This is due to the missing cross section covariance data of ^{236}U in JEFF-3.3.

The uncertainty on the concentration of ^{234}U shows a completely different

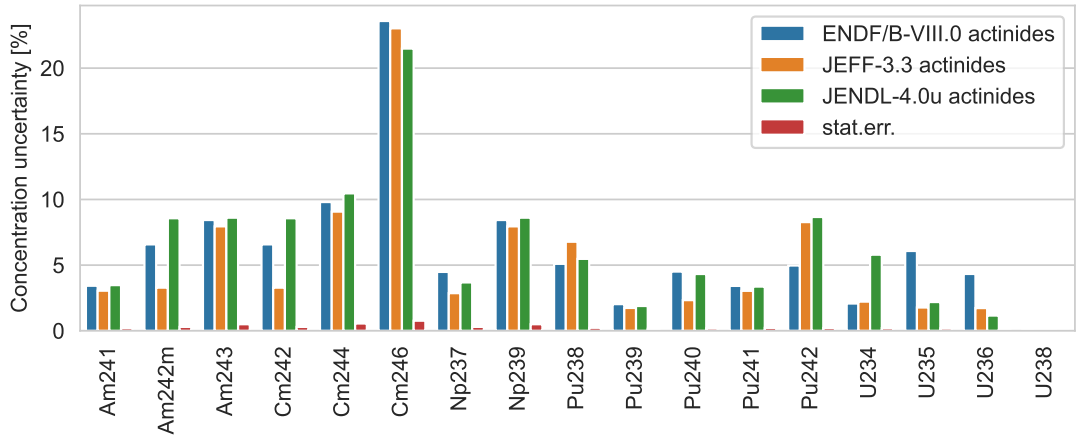

Figure 4.1: Calvert Cliffs MKP109-P: Nuclear data uncertainty on actinide compositions and comparison with the propagated statistical error inherent to the Monte Carlo method.

trend, related to its neutron capture cross section uncertainty differences among the considered nuclear data libraries. These nuclear data uncertainties are of the order of 10% in JENDL-4.0u and of the order of 2% both in JEFF-3.3 and ENDF/B-VIII.0. This uncertainty appears to be basically not propagated to ^{235}U composition. This is to be justified with the ^{235}U production rate in the reactor — which is rather small given the low concentration of ^{234}U and its cross section that is lower than ^{235}U fission one. This is expected to result in low sensitivity of ^{235}U concentration to ^{234}U. The uncertainty trend reported for ^{234}U is justified by the evaluated uncertainty difference in its neutron capture cross section, about twice larger in JENDL-4.0u than in JEFF-3.3 and ENDF/B-VIII.0, which present the same evaluation. The same large uncertainty evaluation — of the order of 50% — is reported in all the considered libraries for ^{234}Th, which is a contributor to the production of ^{234}U through β^- decay chain. The effect of this large uncertainty is not that visible on ^{234}U because of to the short half life of ^{234}Th. Similar discussion would hold for ^{234}Pa, for which no covariance data are given, though. The uncertainty on ^{238}U neutron capture and fission cross sections is too low to have clear effect on the ^{234}U concentration uncertainty, also considering that it is quite far as a precursor ($^{238}\mathrm{U} \xrightarrow{\alpha} {}^{234}\mathrm{Th} \xrightarrow{\beta^-} {}^{234}\mathrm{Pa} \xrightarrow{\beta^-} {}^{234}\mathrm{U}$).

The concentration uncertainty ^{239}Pu is about 2% for each considered library, which is consistent to what was found in the cross section standard deviations. On the other hand, the uncertainties on ^{240}Pu and ^{241}Pu are larger, despite being below 5%. ^{240}Pu neutron capture cross section uncertainty in JEFF-3.3 is twice as small as in the other libraries, which is likely to explain the discrepancy visible in Fig. 4.1.

Despite not having perturbed the cross section data for ^{241}Am, as discussed in section 4.1, the uncertainty results are in quite good agreement among the three libraries. Depending on the standard deviation on ^{241}Am considered in JEFF future versions, this might result in discrepancies. JEFF-4.0 is now being produced and two successive preliminary versions have been evaluated so far (namely, JEFF-4.0t0 and JEFF-4.0t1). Both those evaluations do not provide covariance data for ^{241}Am.

Concerning ^{244}Cm and ^{246}Cm, overall consistency was found among the libraries. This is despite the missing covariance matrices of ^{242}Pu in JEFF-3.3, which are involved in ^{244}Cm production through neutron captures and β^- decay, as reported in Ref. [31]. The uncertainty larger than 20% on ^{246}Cm is overall in agreement with the nuclear data uncertainty. Still it is note-worthy that the same uncertainty evaluation is given both in ENDF/B-VIII.0 and JENDL-4.0u for the neutron capture cross section of ^{243}Cm. Despite this, a difference was found among the results of the two calculations, which is likely to be due to uncertainty evaluation discrepancies along ^{246}Cm production path. Similar discussion holds for JEFF-3.3 uncertainty propagation, as the evaluated standard deviations on the neutron capture and fission cross sections are lower there than in the other libraries. Yet, the effect

of the whole buildup chain results in the concentration uncertainty reported in Fig. 4.1.

4.1.2 Fission products

Both actinides' and fission products' cross sections uncertainties were propagated to fission product concentrations. As a consequence of what was discussed about production paths, one can understand how the effect of fission product capture cross section uncertainty is of major relevance on those nuclides which production happens via neutron captures in other fission products. This is because the uncertainty tends to build up along these creation paths, resulting in this effect. The visibility of such an effect is also increased by the fact that only cross section uncertainties were propagated, whereas other relevant uncertainty sources such as fission yields were not considered in this analysis. Moreover, the lack of evaluated covariance data available in the considered libraries most likely results in an underestimation of the total uncertainty as discussed in section 4.1.

The effect of the actinides' cross section uncertainty on fission product concentrations was found to be negligible overall. This is because many of the fission products under investigations are mainly produced by neutron captures in other fission products, which makes the contribution of actinides' cross section uncertainty less relevant the further the considered nuclide is in the capture chain. For this reason and for the sake of readability, only the uncertainties propagated from ENDF/B-VIII.0 are reported in Fig. 4.2, being the more relevant among the three considered libraries. The results are reported to the time when the measurements were performed or at the time of KRI measurements for the non-measured nuclides.

Here it is also recalled that JENDL-4.0u results are not present in Fig. 4.2 as no covariance data are provided there for fission product cross sections.

Calculations with both JEFF-3.3 and ENDF/B-VIII.0 resulted in concentration uncertainties above 25% in ^{155}Eu and ^{155}Gd. These uncertainties might very well be related as ^{155}Gd is produced by ^{155}Eu β-decay as well as by direct fission, despite the relatively long half life of ^{155}Eu — i.e. about 4 years. The uncertainties on ^{155}Eu concentration are in agreement with its cross section uncertainties. On the other hand, the uncertainties on ^{155}Gd concentration are also affected by the high uncertainties on the concentration of ^{154}Gd, from which ^{155}Gd is produced via neutron capture. As a matter of fact, ^{154}Gd is an end-of-chain fission product, which makes it more likely to accumulate as it is only removed by neutron capture and not by decay. This should have the effect to increase ^{155}Gd concentration uncertainty. Moreover, it should be reported that both ENDF/B-VIII.0 and JEFF-3.3 neutron capture cross section uncertainty evaluations are the same for ^{154}Gd, originating from ENDF/B-VII.1. This highlights how having the same evaluation is not necessarily symptom of better knowledge of the investigated phenomenon, but

could rather even be reflective of limited information. The covariance evaluation for ^{155}Gd neutron capture cross section is not given in JEFF-3.3[2], while its uncertainty evaluated in ENDF/B-VIII.0is approximately half the one evaluated on ^{154}Gd neutron capture cross section. Both ^{155}Eu and ^{155}Gd are present in small quantities in SNF.

The concentration uncertainty of ^{151}Sm presented the largest discrepancy, which results from the large difference in the evaluated uncertainty reported in the considered nuclear data libraries — i.e. of the order of 15% in JEFF-3.3 and of 12% in ENDF/B-VIII.0, when averaged over one group, and goes up until 30% where the neutron spectrum is peaked. Higher uncertainty evaluation in JEFF-3.3 than in ENDF/B-VIII.0 were also encountered in other samarium isotopes, such as ^{149}Sm, which contribution in production paths results in the large difference reported in Fig. 4.2. There, it is also visible the difference in end-of-chain fission products and the other ones. As a matter of fact, the highlighted trend is much more visible for ^{149}Sm and ^{151}Sm than in ^{150}Sm and ^{152}Sm, which are stable. Moreover, the higher evaluated uncertainty of ^{152}Sm neutron capture cross section in ENDF/B-VIII.0 explains the discrepancy compensation on that nuclide.

Uncertainties on ^{133}Cs and ^{134}Cs are of about 1% and 4% respectively. Both JEFF-3.3 and ENDF/B-VIII.0 provide the same evaluation for the uncertainty on ^{133}Cs, which leads to similar considerations as the ones reported above.

All isotopes of neodymium present uncertainties lower than 5%. The uncertainties on ^{148}Nd and ^{137}Cs do not bring any information relevant to the nuclear data because of the power normalisation, being those nuclides linear to the burnup, which is imposed.

The concentration of ^{133}Cs presents about 1% uncertainty. This is lower than the evaluated uncertainty on ^{133}Cs neutron capture cross section, which has the same evaluation both in ENDF/B-VIII.0 and JEFF-3.3. Similarly, ^{134}Cs concentration has uncertainty of about 4%, lower than its evaluated neutron capture cross section uncertainty, which is only given in JEFF-3.3. This is likely due to the low evaluated best estimate value of the neutron capture cross section where the spectrum is peaked, most likely resulting in low sensitivity of the concentration to it.

The calculation ran with ENDF/B-VIII.0 data resulted in higher uncertainty on the concentrations of ^{153}Eu and ^{154}Eu than the one ran with JEFF-3.3 data. The missing evaluation of the covariance matrix of ^{153}Eu neutron capture cross section in JEFF-3.3 is expected to explain this difference in ^{153}Eu concentration, which then propagates to ^{154}Eu through neutron capture production path.

The non-physicality of the evaluated uncertainties on ^{145}Pm in ENDF/B-VIII.0,

[2]A covariance evaluation of ^{155}Gs neutron capture cross section is given in JEFF-4.0t1.

with peaks larger than 1000%, can compromise the calculated concentration uncertainty on samarium isotopes. Despite this, a low sensitivity of samarium isotopes' concentration to ^{145}Pm neutron capture cross section is expected, considering the fact that all the concentration uncertainties of those nuclides computed using ENDF/B-VIII.0 are below 5%.

The predicted concentration uncertainty on the long-lived fission products ^{99}Tc and ^{129}I is approximately 0%.

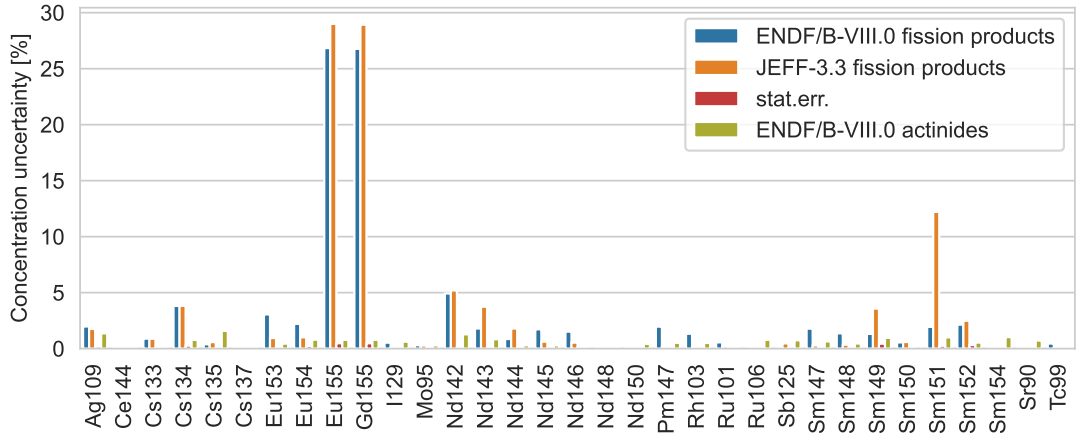

Figure 4.2: Calvert Cliffs MKP109-P: Nuclear data uncertainty on fission product compositions and comparison with the propagated statistical error inherent to the Monte Carlo method.

4.2 Gösgen GU3

The model of Gösgen GU3 is more complex compared to the ones of Calvert Cliffs MKP109-P and Takahama SF95-4, as it requires three successive calculations (one per cycle), given how the model was set up. This makes the uncertainty propagation procedure longer than the one for the other considered benchmarks. Moreover, it was decided to focus this analysis on the discrepancy between the results obtained using JEFF-3.3 and the ones of JEFF-4.0t1, the latest beta-version of the latest upgrade of JEFF nuclear data library. For these reasons, the uncertainty propagation procedure was focused on the fission products, as their covariance data were majorly improved in JEFF-4.0t1. Moreover, the magnitude of the statistical error was not assessed for this benchmark and is left for future studies.

The newly evaluated data in JEFF-4.0t1 were processed at SCK CEN. A posteriori, some errors in this processing were found: the sampling for the cross sections of ^{103}Rh, ^{155}Gd, ^{156}Gd, ^{157}Gd and ^{86}Y. Those data were therefore considered to be with no uncertainty in JEFF-4.0t1, meaning their uncertainty was not propagated.

Nevertheless, some covariance data missing in JEFF-3.3 are given in JEFF-4.0t1. The processing of JEFF-4.0t1 highlighted that the nuclides for which covariance data were added to JEFF-3.3 are isotopes of barium, cerium, dysprosium, gadolinium, molybdenum, neodymium, promethium, antimony, samarium and xenon.

Apart from this, the same considerations reported in 4.1 hold for the uncertainty propagation performed on Gösgen GU3.

4.2.1 Fission products

The fission product concentration uncertainty results are in the line with what reported in section 4.1.2, as displayed in Fig. 4.3. The results are computed at discharge date.

When comparing them with the ones propagated from JEFF-4.0t1, the effect of some changes is visible on a number of nuclides, namely ^{135}Cs, ^{153}Eu, ^{154}Cs, ^{154}Eu, ^{155}Eu, ^{155}Gd, ^{142}Nd, ^{150}Sm, ^{151}Sm, ^{152}Sm. Overall, the uncertainty increase from JEFF-4.0t1 when compared with the one propagated from JEFF-3.3 is a consequence of including more covariance evaluations.

The effect of the larger uncertainty evaluation of the neutron capture cross section of ^{135}Cs is visible in Fig. 4.3. The uncertainty results on the concentration of ^{153}Eu are in line with the ones propagated from ENDF/B-VIII.0 and suggest a change in the covariance evaluation in JEFF-3.3, evolving towards the one of ENDF/B-VIII.0. This effect propagates to ^{154}Eu as well through neutron capture and would most likely result in a larger uncertainty on the concentration of ^{155}Eu as well. This would need to be further investigated in future studies.

The strong decrease in the uncertainty on the concentration of ^{155}Gd is probably

related to the errors in the processing of the covariance data of the neutron capture cross section of ^{155}Gd, being such a large uncertainty mainly originating from that source as discussed in section 4.1.2. The concentration uncertainty of ^{142}Nd change is most likely reflective of a change in its evaluated neutron capture cross section covariance evaluation. This effect propagates to the successive neodymium isotopes through neutron capture. This results in a concentration uncertainty prediction similar to the one from ENDF/B-VIII.0 for many of them. The overall low uncertainty on the concentration of neodymium isotopes is explained by the normalization of the model. The uncertainty discrepancy on the concentration of ^{151}Sm seems to be redistributed to ^{150}Sm and ^{152}Sm in the latest evaluation of JEFF.

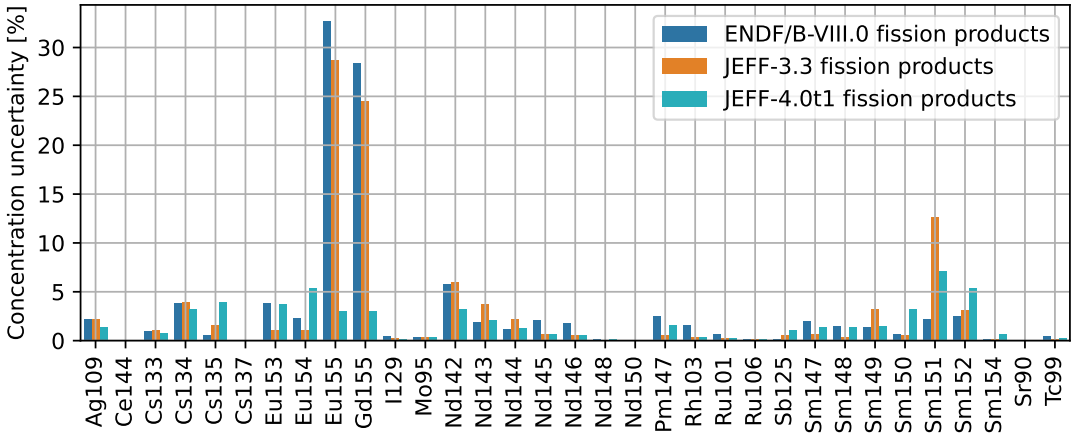

Figure 4.3: Gösgen GU3: Nuclear data uncertainty on fission product compositions.

4.3 Takahama SF95-4

The same uncertainty propagation procedure described in section 4.1 was applied to Takahama SF95-4. Overall, similar results to those reported in section 4.1 were found. This means that the effect of actinides' cross section perturbation on fission products was found to be negligible (of the order of 2% of lower if ENDF/B-VIII.0 is considered). Similar consideration holds when the effect of fission products' perturbation on actinides' concentrations was assessed. The same considerations reported in section 4.1 on this hold here as well.

Because of a larger complexity of the model combined with a lower particle density resulted in overall larger statistical error in these results when compared with the ones obtained for Calvert Cliffs MKP109-P.

When commenting on these discrepancies, one should consider three major causes a part from the irradiation history and other model assumptions, namely the different burnup of the two samples, the different initial enrichment and the different time at which the uncertainty results are reported. This is the measurement time for Calvert Cliffs MKP109-P and the discharge date for Takahama SF95-4. The effect of this is visible only in the comparison of short/medium-lived nuclides and causes an uncertainty decrease in Calvert Cliffs MKP109-P, as there a decay time is included in the results.

Both the burnup difference and the lower initial enrichment — 3.038% wt and 4.1% wt in ^{235}U for Calvert Cliffs and Takahama respectively — play a role in the same direction. This means that the buildup of ^{239}Pu and the depletion of ^{235}U will respectively be larger and smaller in Calvert Cliffs MKP109-P than in Takahama SF95-4.

The analysis of the uncertainty results for Takahama SF95-4 are also complemented with a comparative analysis on the concentration uncertainty evolution with burnup. The results for the analysed samples of Calvert Cliffs and Takahama burnup evolution, reported in section 4.4, was considered to be needed to explain some of the discrepancies reported in the following. The analysis reported in section 4.4 was then extended to all the nuclides in the considered set, presenting noticeable differences either comparing the nuclear data libraries either the two benchmarks.

4.3.1 Actinides

The difference in ^{241}Am concentration uncertainty is reflective of the fact that its cross sections were not perturbed in this analysis. This was not visible in the results presented in section 4.1.1 because of the decay time included there, during which ^{241}Am is still produced by ^{241}Pu β^- decay (being the half life of ^{241}Pu $\approx$ 14 y). This is showed in Fig. 4.10, in section 4.4.

The decay time considered for sample Calvert Cliffs MKP109-P also explains the lower uncertainty of ^{239}Np concentration found in Takahama SF95-4, as the decay of ^{239}U, whose half life is rather short — about 23 min —, increases it.

The larger uncertainty in ^{244}Cm concentration found in Takahama SF95-4 is mainly due to the lower burnup of the sample. As a matter of fact, for many minor actinides the concentration uncertainty shows a decreasing trend as reported in section 4.4. The same holds for ^{246}Cm.

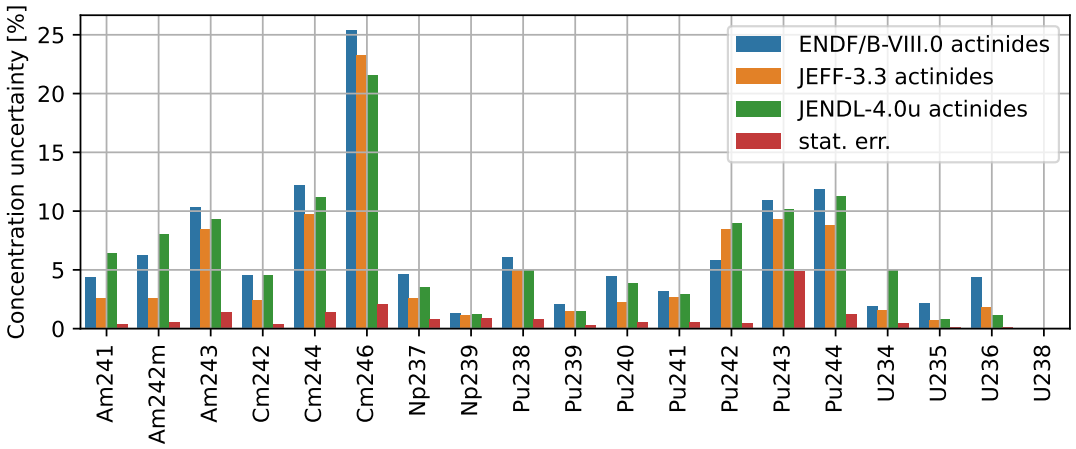

Figure 4.4: Takahama SF95-4: Nuclear data uncertainty on actinides compositions and comparison with the propagated statistical error inherent to the Monte Carlo method.

4.3.2 Fission products

The main discrepancy concerning the concentration uncertainty of fission products. A larger uncertainty in ^{155}Eu concentration was found in Takahama SF95-4. This is a result of the larger enrichment of this sample and of the lower cumulative fission yield of ^{155}Eu from ^{235}U fission than from plutonium isotopes — mainly ^{239}Pu. An evaluation for the uncertainty of ^{153}Eu neutron capture cross section is given in ENDF/B-VIII.0 and not in JEFF-3.3. This builds up from ^{153}Eu to ^{155}Eu through successive neutron captures. The sensitivity to this uncertainty then decreases as the fission yield of ^{155}Eu increases, resulting in a larger sensitivity to its own neutron capture cross section, for which the evaluation is larger in JEFF-3.3 than in ENDF/B-VIII.0. This explains the difference in the propagated uncertainty from the different libraries at different burnup that emerges comparing Fig. 4.4 to Fig. 4.1.

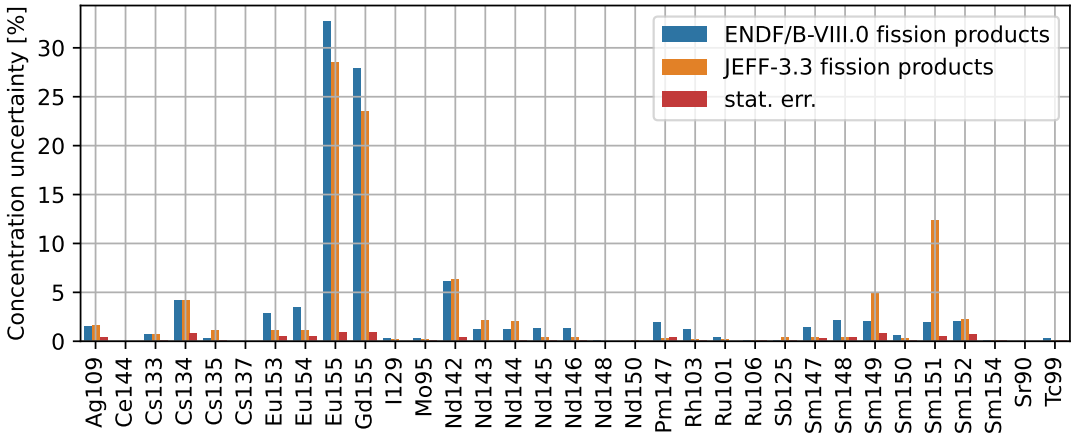

Figure 4.5: Takahama SF95-4: Nuclear data uncertainty on fission product compositions and comparison with the propagated statistical error inherent to the Monte Carlo method.

4.4 Burnup-dependent uncertainty analysis

In this section, an analysis of the evolution of the uncertainty during the irradiation time is reported. In general, different contributions to the uncertainty have different relevance at different irradiation levels. This is because changing the fuel composition with burnup, some production paths of certain nuclides gain in relevance while other loose relevance. A clear example of this is the fission products of plutonium isotopes. No plutonium is present in the fresh fuel, therefore ^{235}U and ^{238}U fission yields are the only source of fission products. This changes with the increase of burnup as ^{239}Pu and ^{240}Pu build up and contribute to the fissions up until when they become the main contributors. At this last stage, their fission yields will be the main paths to produce the primary fission products.

In the following, the results for Takahama and Calvert Cliffs are compared. The comparison of these two benchmarks is particularly suitable as those both referred to PWR. The effect of gadolinium-enriched rods in the assembly of Takahama will affect the spectrum making it harder. On the other hand, the larger amount of ^{235}U — i.e. 4.1 wt.% initial enrichment, compared to the 3.038 wt.% one of Calvert Cliffs — contribute to make ^{239}Pu and ^{240}Pu fissions more relevant in Calvert Cliffs than in Takahama, which in turn results in a hardening of the spectrum in Calvert Cliffs.

The sensitivity analysis reported in [31] at different burnup is the main reference for the interpretation of the results reported in this section. There, the effect of the different normalisation considered for the simulations is also reported. This is of major importance for the reported analysis and more in general for such uncertainty studies and propagation through MC reactor physics models, as it highlights that an *artificial* correlation is introduced by the normalisation. This means that the sensitivity of ^{235}U concentration to ^{239}Pu will be not negligible even if ^{235}U is almost not produced in the reactor, and certainly not directly produced by ^{239}Pu. This means that non-negligible non-physical correlations might affect the results of the uncertainty propagation performed. No more detail is given on this as no simulation with different normalisation was run. Yet, an analysis of the effect of considering a flux normalisation on these benchmarks could be of interest for future studies.

A few other general considerations are worth reporting before diving into the analysis of the most interesting trends resulting from the study. On the one hand, the concentration of nuclides with short half lives — i.e. half life $\lesssim 3$ days — goes to zero during the refueling operation. This reduces their uncertainty to zero, which makes the comparison of the two benchmarks meaningless as the refueling was of course not synchronous. On the other hand, the statistical error tends to be larger the smaller the concentration of the nuclides under analysis. An example of this is given in Fig. 4.11, where the burnup dependency of the uncertainty and of the

statistical error is reported for ^{103}Rh. There, the important role of the statistical error compared to the one propagated from the cross sections at low burnup is also visible. This means that the statistical error on ^{235}U concentration will start from 0 and grow with ^{235}U depletion, while the statistical error of fission products in general decreases with burnup as they accumulate. This concept will be recalled when analysing the differences in the uncertainty built up in the first irradiation steps. Finally, bearing in mind the order-of-magnitude approach to the uncertainty quantification, even discrepant trends at low uncertainties are not reported.

Overall, a larger prediction of the concentration uncertainty was found in ENDF/B-VIII.0, which is consistent to its generating idea, which is to give conservative uncertainty evaluations as reported in [4].

4.4.1 Analysis of the most noteworthy trends

The uncertainty on ^{235}U was found to be lower in Takahama SF95-4 sample than in Calvert Cliffs MKP109-P one.

The large variation of the concentration uncertainty evolution trend of ^{235}U from Takahama to Calvert Cliffs highlights its sensitivity to the importance of ^{239}Pu and ^{241}Pu fissions. As a matter of fact, Fig. 4.6 reports a larger ^{235}U concentration uncertainty at lower enrichment (Calvert Cliffs) and increasing with the sample burnup. This effect comes both from the *artificial* correlation of these two nuclides induced by the power normalisation[3] and from the reduction in ^{235}U concentration in the sample, which will be almost completely consumed at end of irradiation. Despite the trend being similar for all the considered libraries, ENDF/B-VIII.0 predicts a larger uncertainty on ^{235}U concentration as a consequence of the larger uncertainty evaluated there for the fission cross section on ^{239}Pu.

The production of ^{237}Np can happen either via (n, 2n) reactions in ^{238}U either via capture and β^- decay from ^{236}U. The uncertainty on the cross section of the first reaction mentioned is larger in ENDF/B-VIII.0, while the latter has larger evaluated uncertainty in JENDL-4.0u. These two effects seem to compensate each other resulting in similar uncertainties propagated from both libraries. The uncertainty of the neutron capture cross section of ^{237}U is only evaluated in JENDL-4.0u, but this should not have a large impact on ^{237}Np concentration considering the short half life of ^{237}U — approximately 7 days. The lower prediction

[3]When normalizing to the sample burnup, one is setting the energy generated in the fuel sample itself. Therefore, all the energy production means in the fuel sample will be correlated by such a normalization constraint. As a result, the number of fissions happening in uranium and plutonium isotopes is not a free parameter, being linked to the sample burnup. This correlation is what is referred to as *artificial* correlation of ^{235}U and ^{239}Pu, which are the most relevant fissioning nuclides.

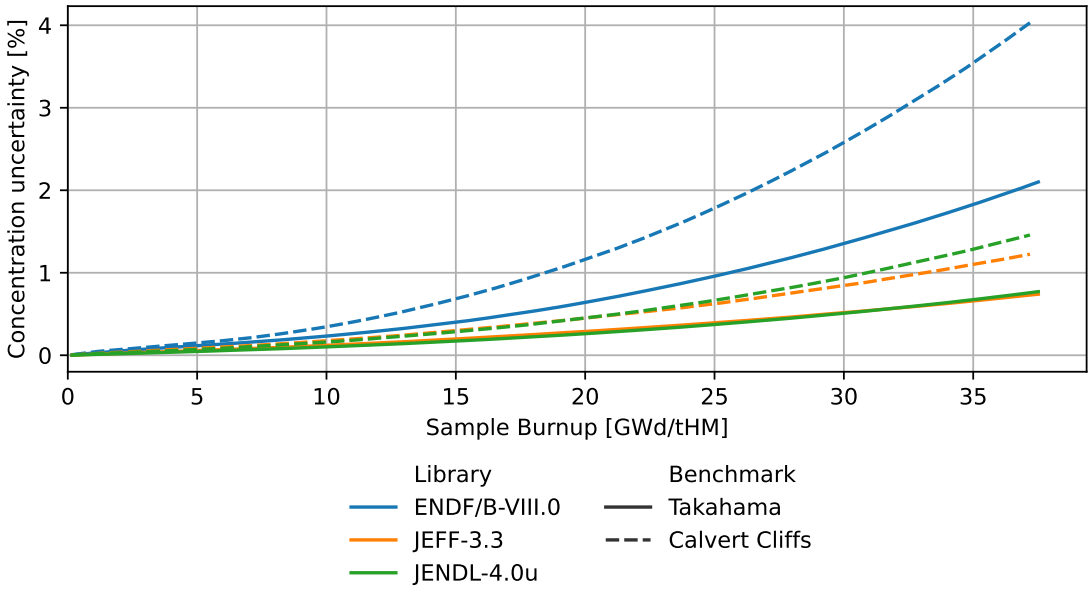

Figure 4.6: Evolution of the uncertainty of ^{235}U concentration with burnup.

of the uncertainty given by the propagation of the cross section uncertainties in JEFF-3.3 is likely to be due to the missing covariance matrix of ^{236}U.

The overall trend of ^{237}Np concentration reminds of the one of plutonium isotopes in FIG. 4.9, which is possibly propagated to ^{237}Np through α decay of ^{241}Am.

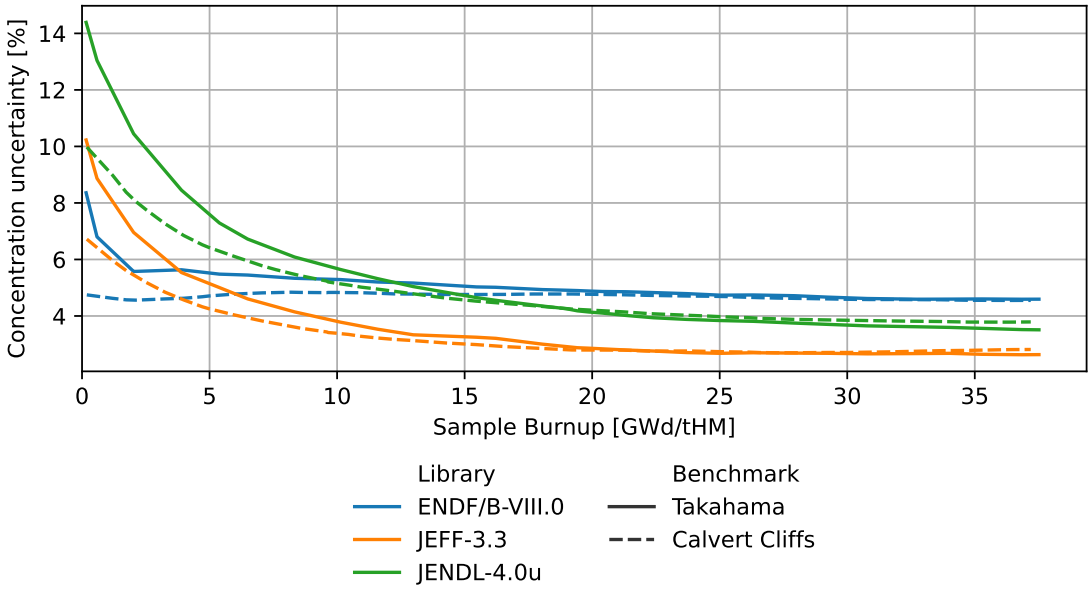

Figure 4.7: Evolution of the uncertainty of ^{237}Np concentration with burnup.

As reported in Ref. [31], ^{238}Pu builds up following three main paths, in order of relevance:

1. $\ldots \rightarrow {}^{236}\mathrm{U} \xrightarrow{(n,\gamma)} {}^{237}\mathrm{U} \xrightarrow{\beta^-} {}^{237}\mathrm{Np} \xrightarrow{(n,\gamma)} {}^{238}\mathrm{Np} \xrightarrow{\beta^-} {}^{238}\mathrm{Pu}$
2. ${}^{238}\mathrm{U} \xrightarrow{(n,2n)} {}^{237}\mathrm{U} \xrightarrow{\beta^-} {}^{237}\mathrm{Np} \xrightarrow{(n,\gamma)} {}^{238}\mathrm{Np} \xrightarrow{\beta^-} {}^{238}\mathrm{Pu}$
3. $\ldots \rightarrow {}^{241}\mathrm{Am} \xrightarrow{(n,\gamma)} {}^{242g}\mathrm{Am} \xrightarrow{\beta^-} {}^{242}\mathrm{Cm} \xrightarrow{\alpha} {}^{238}\mathrm{Pu}$

Considering the amount of minor actinides involved in the production of ^{238}Pu, the effect of the correlation introduced by the normalisation is expected to be larger for this nuclide, which presents a negative sensitivity to the fissions in ^{235}U as reported in figures 6 and 7 in [31]. JENDL-4.0u evaluates a larger uncertainty on ^{236}U neutron capture cross section than ENDF/B-VIII.0, around 5% with a peak above 30%, compared to the approximately 4% in ENDF/B-VIII.0. The covariance matrix of ^{236}U is not given in JEFF-3.3. ENDF/B-VIII.0 also evaluates a larger uncertainty of the (n,2n) reaction of ^{238}U close to its threshold energy — of the order of 40% —, which makes ENDF/B-VIII.0 give the larger prediction of the uncertainty on the

concentration of ^{238}Pu, as reported in Fig. 4.8. The same uncertainty evaluation is given in ENDF/B-VIII.0 and in JENDL-4.0u for the neutron capture cross section of ^{242}Cm, of the order of 15%, while JEFF-3.3 evaluated it to be above 20%. This, combined to the lower enrichment of Calvert Cliffs, explains the rise in the uncertainty in ^{238}Pu propagated from JEFF-3.3, reported in Fig. 4.8.

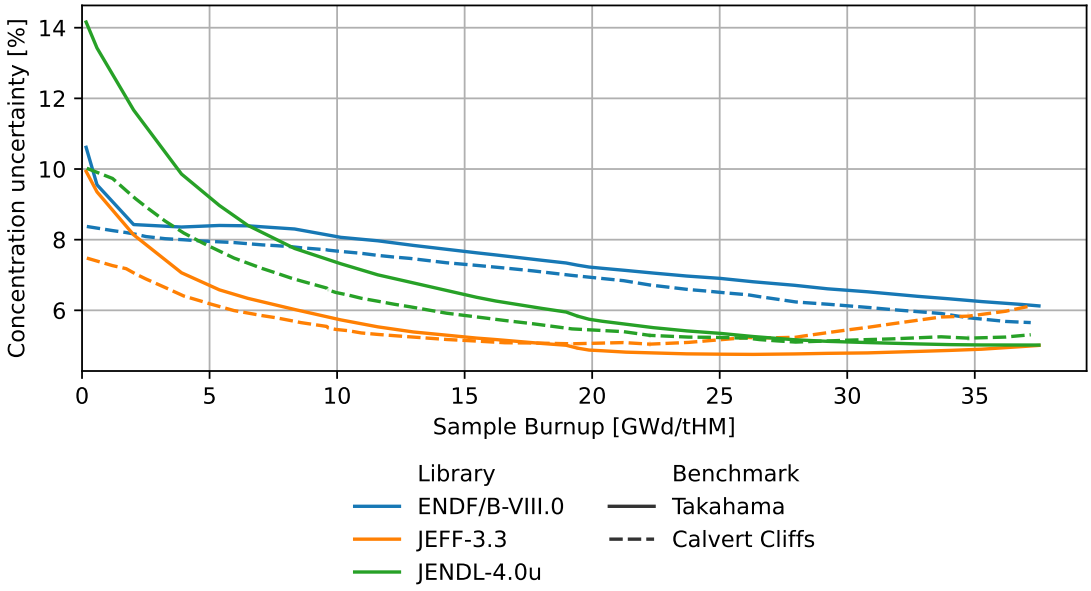

Figure 4.8: Evolution of the uncertainty of ^{238}Pu concentration with burnup.

The concentration uncertainty evolution with burnup of several other plutonium isotopes is reported in Fig. 4.9. These were grouped because of shared production paths, starting from the neutron captures in the resonances of ^{238}U cross section. The uncertainty of ^{239}Pu concentration is overall rather small when compared to the other plutonium isotopes. The many nuclides and reactions that are relevant for this uncertainty to build up and the statistical error of the order of 1%, combined with uncertainty evaluations of the same order of magnitude in all the considered nuclear data libraries and with the correlation introduced by the normalisation, make it hard to give a clear interpretation of the trend, especially at low burnup. Yet, the buildup of plutonium isotopes increases the sensitivity of the concentration uncertainty to the uncertainties on their cross sections, which might be the reason behind the increasing trend of the uncertainty at larger burnup for ^{239}Pu.

The ^{240}Pu neutron capture cross section uncertainty evaluated in JENDL-4.0u is larger than the ones from the other nuclear data libraries, above and below 5% respectively, which is coherent with the increasing trend with burnup — i.e. with ^{240}Pu buildup — reported in Fig. 4.9. The overestimation given by ENDF/B-VIII.0 with

respect to the other libraries is likely to come from ^{239}Pu.

The uncertainties on ^{241}Pu decrease converging to a value around 2%. The same considerations on ENDF/B-VIII.0 hold and the trend is consistent with what it is reported for ^{241}Am, especially at low burnup — i.e. lower sensitivity to ^{241}Am cross section uncertainties, as reported in Fig. 4.10.

Overall, the uncertainty on plutonium isotopes results to be poorly affected by the analysed change in initial enrichment.

The low concentration of ^{241}Am at low burnup explains its larger uncertainty during the first irradiation steps. Later, until approximately 20 $\frac{\text{GWd}}{\text{tHM}}$, ENDF/B-VIII.0 overestimates the uncertainty of ^{241}Am when compared to the other nuclear data libraries, as reported in Fig. 4.10. This is coherent to what it is reported in Fig. 4.9 for the precursors of ^{241}Am and is relevant until when the concentration of ^{241}Am itself makes its uncertainty more sensitive to its own cross sections.

The main reaction of ^{241}Am is neutron radiative capture and the evaluated uncertainties for both its neutron capture cross section and fission cross section are of the same order of magnitude. Yet, the larger uncertainty evaluated by JENDL-4.0u for the ^{241}Am neutron capture cross section at energies above 0.1 eV justifies what is reported in Fig. 4.4, where larger concentration uncertainty prediction is reported for JENDL-4.0u than for ENDF/B-VIII.0. This effect on the predicted concentration uncertainty becomes even more relevant at larger burnup[4], because of the buildup of ^{241}Am and as an effect of the spectrum hardening. The cross section of ^{241}Am in JEFF-3.3 was not perturbed, which is coherent to what reported in Fig. 4.10.

[4]The buildup of plutonium isotopes in the fuel happens with the fuel burnup. This makes the spectrum harder because of the neutron capture and fission cross section resonances at about 1 eV and beyond, typical of plutonium isotopes.

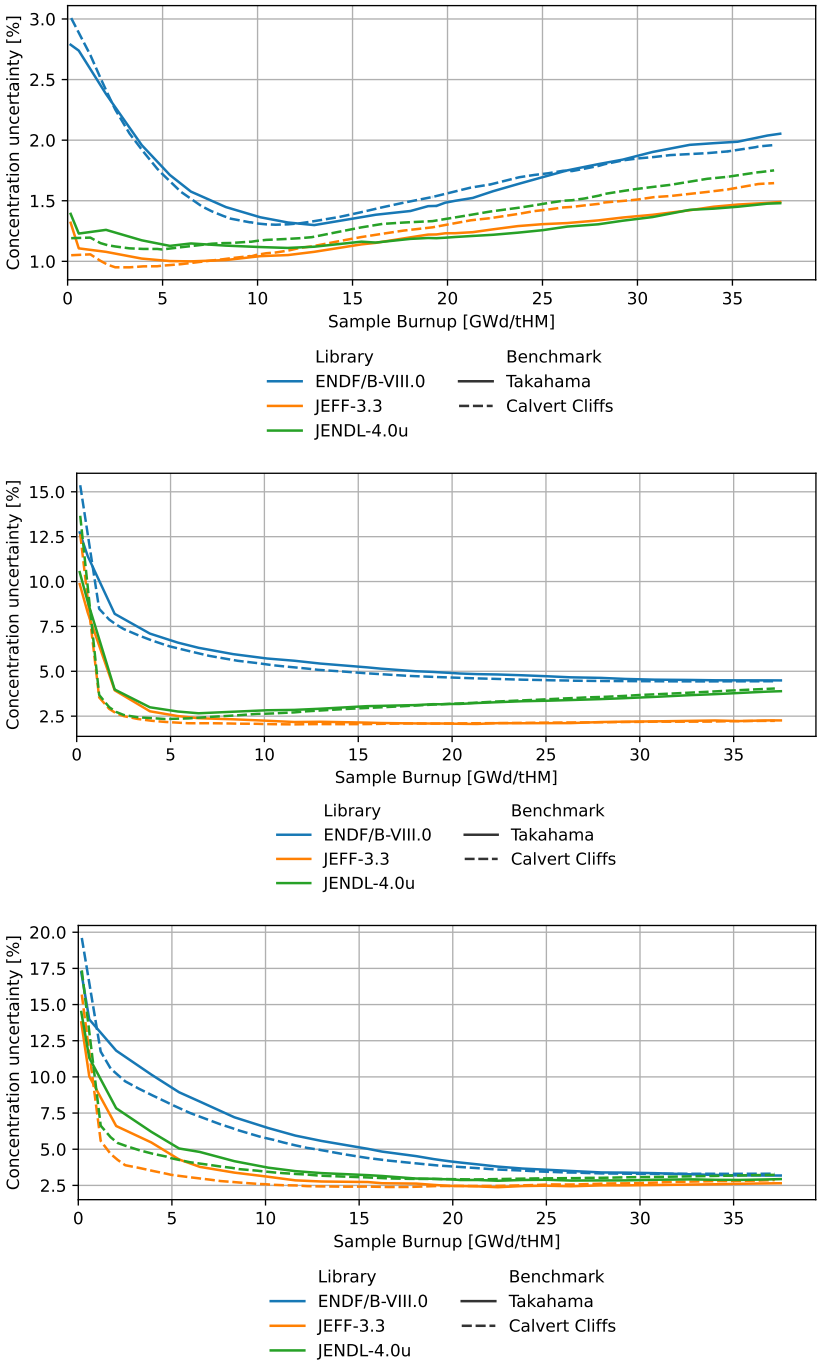

Figure 4.9: Evolution of the concentration uncertainty of several plutonium isotopes with burnup.

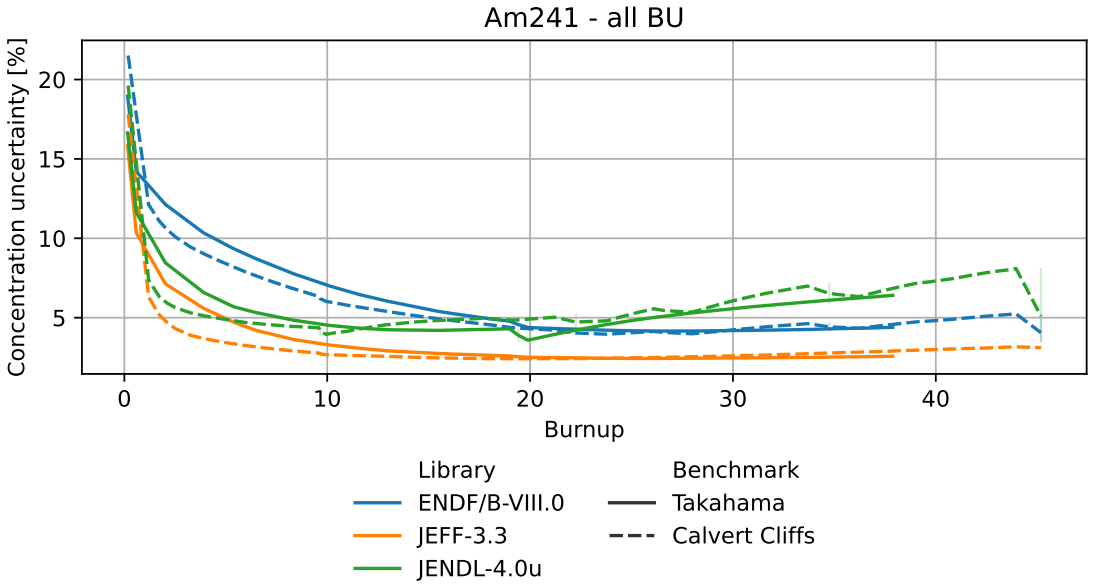

Figure 4.10: Evolution of the uncertainty of ^{241}Am concentration with burnup.

Concerning the fission products, the statistical error has overall a larger impact on the concentration uncertainty, given the low concentration of many fission products, especially at low burnup.

From Fig. 4.11, the uncertainty on the concentration of ^{103}Rh seems to be minimally affected by the change in the enrichment, which results from the similar fission yield of nuclides with atomic mass 103 uma from ^{235}U, ^{239}Pu and ^{241}Pu. The lower prediction of the uncertainty from JEFF-3.3 is attributable to the error in the processing of the covariance data for the neutron capture cross section of ^{103}Rh in JEFF-3.3.

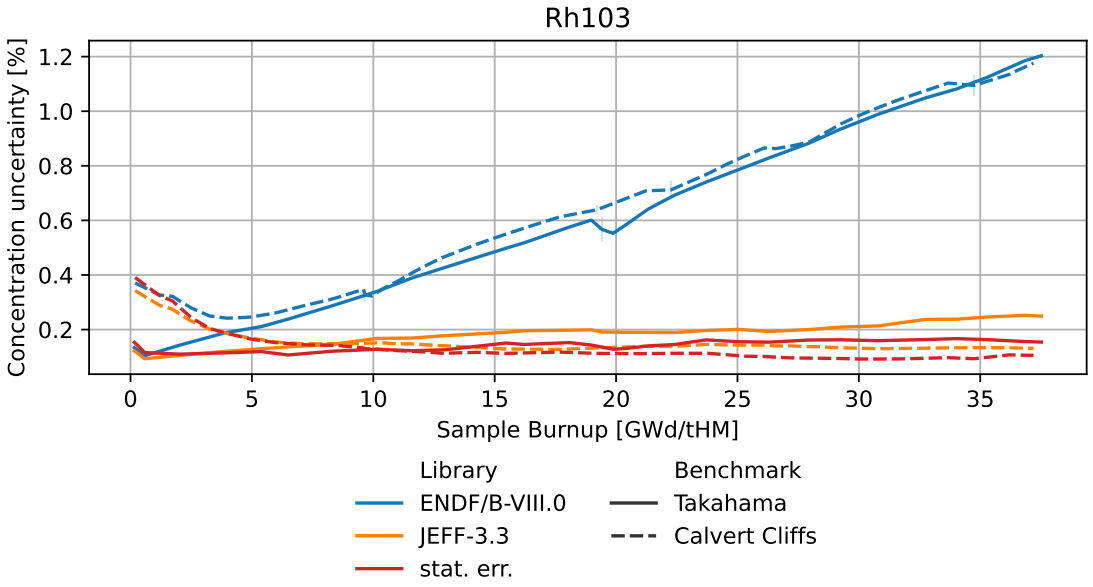

Figure 4.11: Evolution of the uncertainty of ^{103}Rh concentration with burnup compared with the related statistical error.

Similarly to what was discussed for the uncertainty on the concentration of ^{103}Rh, the concentration uncertainty of ^{147}Pm is larger in ENDF/B-VIII.0 than in JEFF-3.3, as reported in Fig. 4.12. This comes from the fact that ENDF/B-VIII.0 gives evaluations for the uncertainties of the neutron capture cross sections of many of promethium isotopes.

Fission yield difference effects are reported for ^{142}Nd and ^{143}Nd, which present different fission yields when comparing ^{235}U and the fissionable plutonium isotopes. The evaluated uncertainties on ^{142}Nd and ^{143}Nd are larger in JEFF-3.3 than in ENDF/B-VIII.0, which explains the differences in Fig. 4.13.

Overall, more fission products covariance data are given in JEFF-3.3 than in ENDF/B-VIII.0. This means that more cross sections were perturbed from the

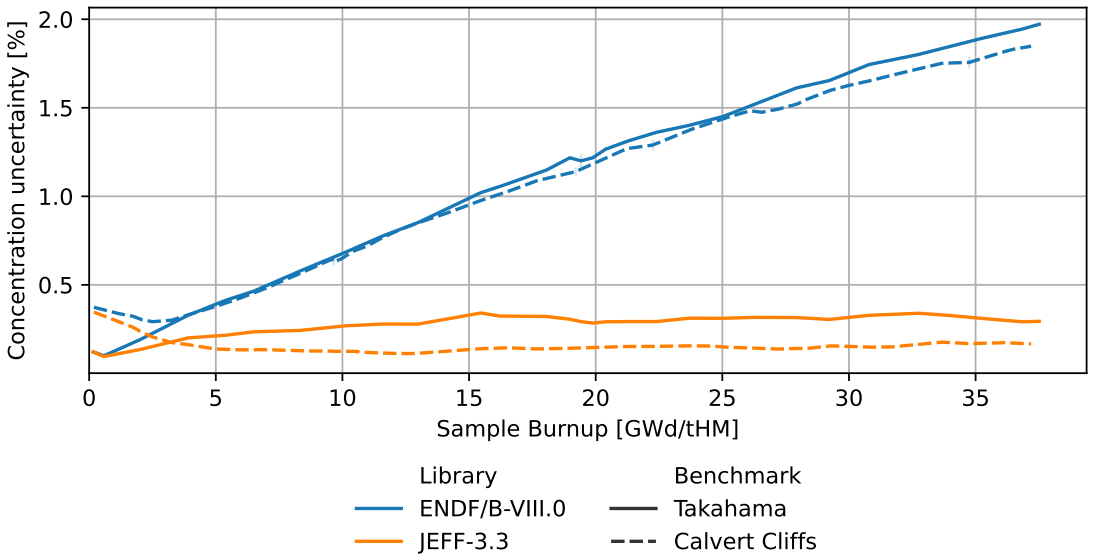

Figure 4.12: Evolution of the uncertainty of ^{147}Pm concentration with burnup.

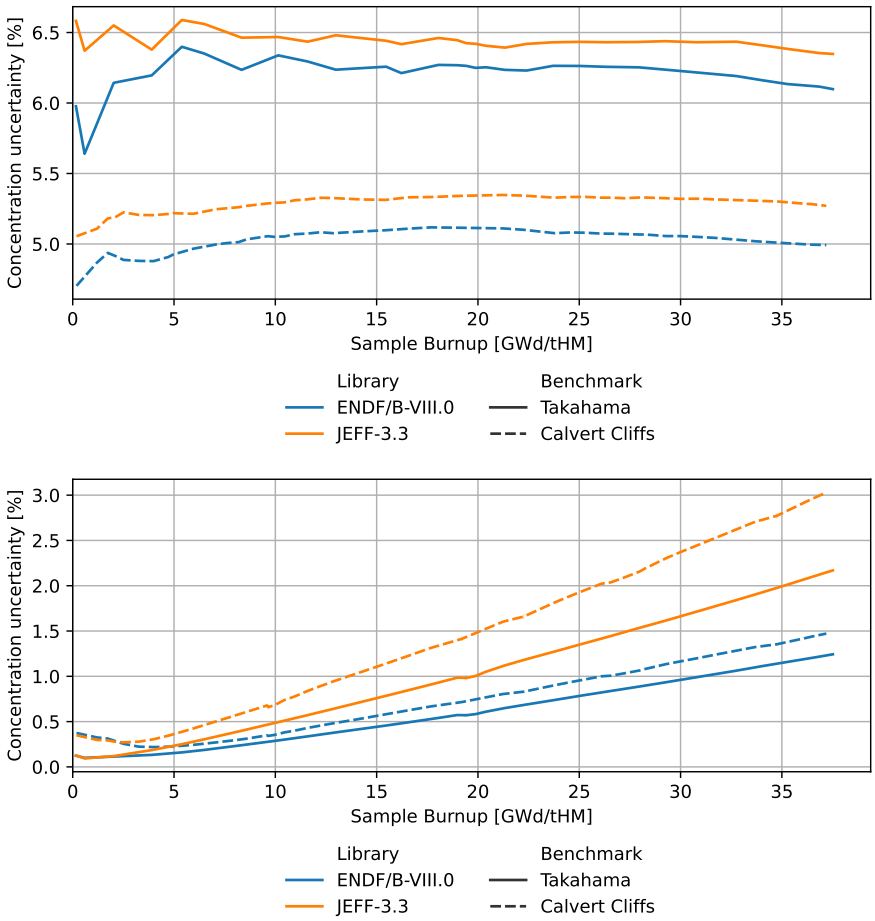

Figure 4.13: Evolution of the the concentration uncertainty of several neodymium isotopes with burnup.

first source than from the latter. Among the nuclides for which more covariance data are given in JEFF-3.3 than in ENDF/B-VIII.0 there are the isotopes of samarium. On the one hand this is not really coherent with what reported in figure FIG. 4.14 for ^{148}Sm, where the conservative approach of ENDF/B-VIII.0 seems to be the reason behind the different prediction. On the other hand it allows for more detailed sensitivity analysis, which seems to be needed to understand what reported in FIG. 4.14. Similarly, some form of ANOVA should be needed to explain the behaviour of ^{152}Sm uncertainty, while the fact that the one propagated from JEFF-3.3 is larger than the one from ENDF/B-VIII.0 is explained by the generally slightly larger uncertainties of ^{152}Sm and ^{152}Sm in JEFF-3.3. The inconsistent trend of the uncertainty might result from the different uncertainty on ^{149}Sm. As a matter of fact, ^{149}Sm concentration reaches a steady state value before 5 $\frac{\text{GWd}}{\text{tHM}}$ burnup and so does the uncertainty. Such an uncertainty is much larger when propagated from JEFF-3.3. Moreover, the concentration uncertainty of ^{151}Sm is larger in JEFF-3.3 than in ENDF/B-VIII.0. A possible change of the sensitivity of the concentration of ^{152}Sm to the cross sections of other samarium isotopes, might explain the peak in FIG. 4.14.

The uncertainty concentration on ^{153}Eu is both reflective of the propagation of the concentration uncertainty of ^{152}Sm for JEFF-3.3 and of the missing covariance data in JEFF-3.3 for the neutron capture cross section of ^{153}Eu. This larger uncertainty seems to propagate from ^{153}Eu to ^{154}Eu, which should have opposite sensitivity to the neutron capture cross section of ^{153}Eu. This is reported in FIG. 4.15.

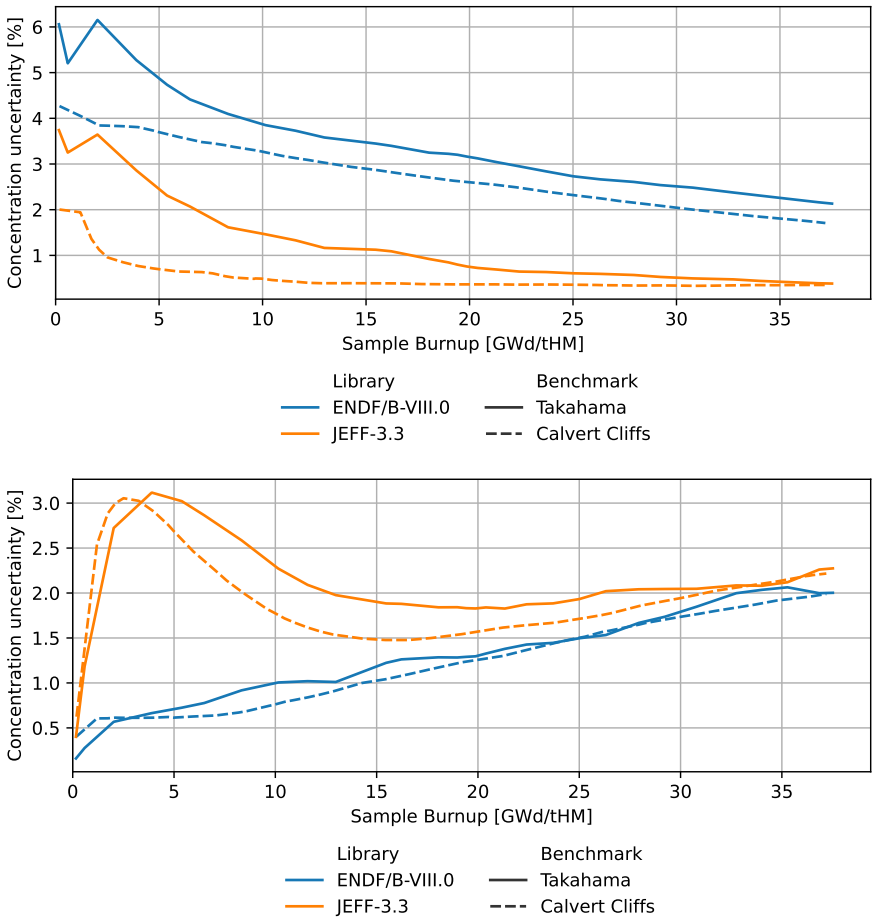

Figure 4.14: Evolution of the the concentration uncertainty of several samarium isotopes with burnup.

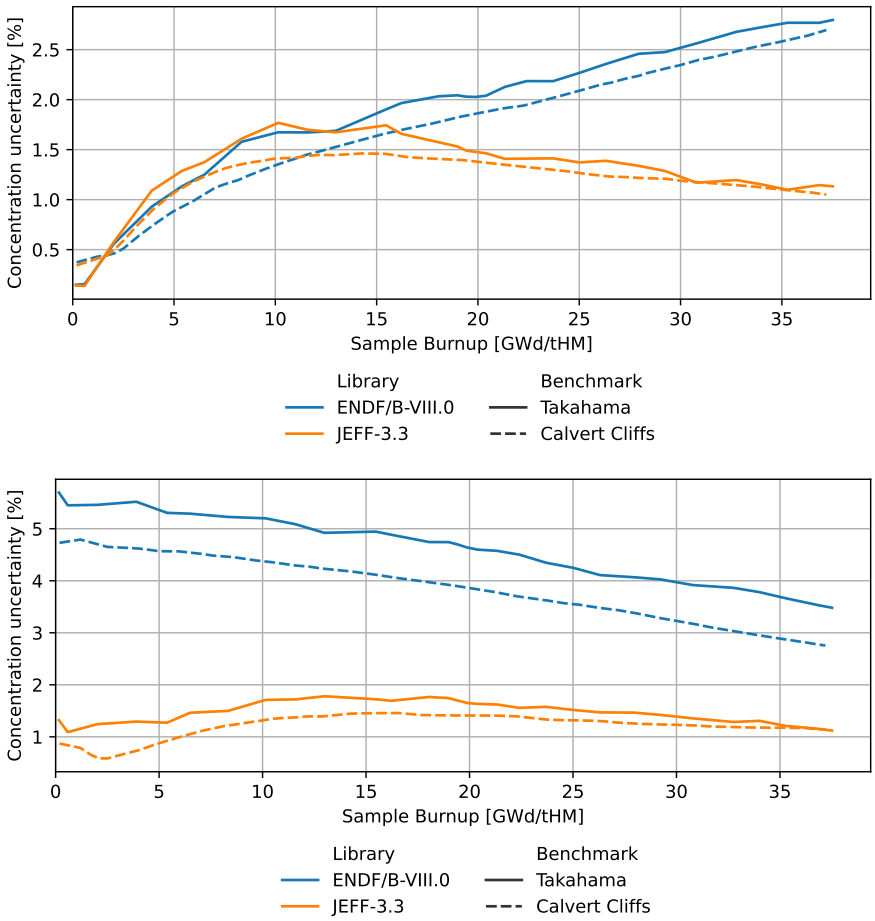

Figure 4.15: Evolution of the the concentration uncertainty of several europium isotopes with burnup.

Chapter 5

Conclusions and future work perspectives

The uncertainty on the cross section of several nuclides was propagated to the inventory of three SNF samples on which experimental composition assessment was performed. The nuclear data from several libraries were considered in doing this (JEFF-3.3, JEFF-4.0t1, ENDF/B-VIII.0, and JENDL-4.0u).

In order to perform statistical sampling-based uncertainty propagation, two models were developed in Serpent for each of the benchmarks describing the assemblies where the analysed samples were irradiated (Calvert Cliffs MKP109-P, Gösgen GU3 and Takahama SF95-4).
The results of the accurate model proved to be in line with the experimental one, almost always being in the range of *two-sigma-deviation* from those. Some measurement errors are likely to justify at least some of the more discrepant values. The accurate models designed to produce those results were then simplified in order to reduce their running time. The same simplifications were implemented for all the benchmarks, resulting in a satisfactory agreement with the accurate model results. Yet, a different impact of the same simplifications was notices, which is reflective of the differences in the model design which makes it differently sensitive to the implemented changes. Assuming a more general perspective, the description of the specific measured sample is not as important as the description of a PWR-like irradiation. This means that for the sake of nuclear data library comparison, what is important is to reproduce in the model the sensitivities typical of a PWR. The uncertainty was then propagated using these simplified models, to which perturbed cross section data were input. The model of Gösgen GU3 was also modelled in ALEPH. The very good agreement of the results contributed to ALEPH validation.

The concentration uncertainties computed on the three considered models show very similar trends. This suggests that the similarities in the three models — i.e.

fuel type, moderator, spectrum, ... — are more relevant in terms of uncertainty propagation mechanism than the differences in initial enrichment and irradiation history. Such a result, strengthens the considerations on designing models representative of PWR-like situations.

The uncertainty propagation resulted in overall good agreement of the sample inventory prediction uncertainty with different evaluated nuclear data libraries. Despite this, the effect of missing covariance evaluations was found to be a cause of uncertainty underestimations in several cases. Overall, ENDF/B-VIII.0 was often found to give larger concentration uncertainties. This results in the conservative approach considered in the evaluation of such a nuclear data library and is reflected on the uncertainty results despite the covariance evaluations being given for more fission products in JEFF-3.3 and JEFF-4.0t1.

Overall, the contribution of the statistical error and of the uncertainty propagated from the fission products was found to be negligible on the concentration uncertainty of the actinides. This resulted in uncertainty predictions of the order or below 20%, with a tendency to an increasing trend with the mass number of the nuclide (i.e. with the neutron capture). The concentration uncertainty of the fission products is more affected by the statistical error, but it is still a minor contribution. The uncertainty propagated from the actinides' cross section to the fission products' concentration resulted to be lower than the one propagated from the cross sections of the fission products. This results from the capture mechanism creating many fission products. Therefore, capture-produced fission products are overall characterised by larger uncertainty. The fission products' cross section uncertainty evaluated in JEFF-4.0t1 was propagated through the model of Gösgen GU3. Some errors in the production of some samples make it hard to have a conclusive statement on the comparison with JEFF-3.3. Yet, the latest evaluation predicts larger uncertainties on the concentration of cesium and europium isotopes, while the predictions of samarium isotopes' concentration uncertainty are more homogeneous.

In order to go deeper in the understanding of the mechanisms that contribute to the concentration uncertainty buildup, a burnup-dependent analysis was also performed. In this frame, the results computed for Calvert Cliffs MKP109-P and Takahama SF95-4 were compared. Differences both due to the different initial enrichment of the two samples and to the different nuclear data covariance evaluation considered were found. The comparison was performed up until 36.69 $\frac{\text{GWd}}{\text{tHM}}$, the sample burnup of Takahama SF95-4, namely. Many propagated uncertainties were found to saturate to asymptotic values. This analysis also highlighted that the different relevance of different uncertainty buildup paths when different nuclear data evaluations are considered. Moreover, a model-induced correlation of the fissile nuclides (mainly ^{235}U and ^{239}Pu), which results from the normalisation of the MC simulation.

The analyses performed allowed to understand the relevance of the nuclide

production mechanism to the concentration uncertainty buildup. Moreover, the effect of missing evaluations was reported to be often relevant, which means that a lower concentration uncertainty prediction doesn't necessarily reflect a better knowledge. This highlights the need of producing improved nuclear data libraries with more and more consistent covariance evaluations. This was found to be happening in the development of JEFF-4.0t1. To conclude, it emerges that an overall overestimation of the uncertainty evaluated for some nuclear data does not allow to decouple the different phenomena that contribute to the uncertainty buildup and subsequently to improve the nuclear data knowledge with new experiments and evaluations.

Finally, some considerations on the uncertainties on the concentration of the nuclides of interest for SNF can be drawn: apart from the concentration of nuclides relevant for neutron emission, the predicted concentration uncertainty is of the order of 10% or below, depending on the considered nuclear data library. The predicted concentration uncertainty on the long-lived fission products is even below 1%, when the nuclides reported in Tab. 1.2 are considered. The concentration uncertainty of the nuclides relevant for neutron emission is larger, being of the order of 30%, mainly because of the uncertainty on curium isotopes. This should be taken into account when considering improvements in the evaluated nuclear data library aiming at better SNF composition description oriented towards the SNF observables, as, depending on the sensitivities of the observables to the nuclide concentrations, nuclear data can be a relevant uncertainty source.

In the presented work, only the evaluated uncertainty on the cross section was propagated. This of course leaves many uncertainty sources out of the scope of the thesis, which should be analysed in future works. Mainly, the propagation of the fission yield and decay data analysis would be of interest and enabled by the version of SANDY under development. Moreover, an analysis of the bias introduced by the choice of the sampling distribution and by the possible inherent standard deviation reduction should be analysed. A contribution to SANDY development was given in this sense. A propagation of the uncertainty on the operational parameters and on the other model input should be considered as well as the inclusion of the covariance data that had processing errors, mainly from JEFF-4.0t1. On same line, the effect of the statistical error on the results obtained for Gösgen GU3 is left to be assessed. Moreover, a more accurate study of the convergence of the results with the number of samples considered would be of interest. One other possible relevant complement of this study would be an analysis of the normalisation constraint choice on the uncertainty propagation and on its evolution with burnup, which was only briefly mentioned in section 4.3.

On a broader perspective, a more consistent comparison of the results from the three (and including more) benchmarks should be considered. This is because the

results proved to be quite consistent in trend and often differentiated by the different initial enrichment. A sensitivity comparative study could be a first needed step in this sense, as well as analysis of the correlation of the resulting concentration distributions. Such studies could confirm the impression that the uncertainty propagation mechanisms in PWR reactors are quite similar from facility to facility and from sample to sample, resulting in the possibility to transfer at least part of the information form one test case to another (and to real applications) and to design meta-models for the nuclear data uncertainty propagation in PWR reactors.

Appendix A

On how the burnup is computed in Serpent

As discussed in section 2.1.4, the burnup problem solution requires the coupling of the transport and depletion problems. In Serpent, the power is computed differently in solving the two problems, which might result in inconsistencies due to the number of neutron histories and batches considered in the simulation.

Being C the normalisation coefficient, Σ_f the fission cross section, E_f the energy released per fission, ϕ the neutron flux and φ the non-normalised one, then the power of each transport calculation P_T — i.e. the power of each batch calculation — will be as reported in Eq. (A.1), where P_{given} is the input power of the simulation.

$$P_T = C\varphi\Sigma_f E_f = \phi\Sigma_f E_f \rightarrow P_{given} \tag{A.1}$$

While the depletion calculation considers one-group-averaged flux and cross section, namely ϕ_{1G} and $\Sigma_{f\,1G}$. Therefore, the power computed in the depletion problem P_D will be as in Eq. (A.2).

$$P_D = \phi_{1G}\Sigma_{f\,1G}E_f = (C\varphi)_{1G}\,\Sigma_{f\,1G}E_f \tag{A.2}$$

The power given by Serpent is the batch-wise average of P_T, $< P_T >$ from now on. Considering C and E_f constant, which is the case for a single fissioning nuclide, P_D will equal $< P_T >$ only if

$$< \phi\Sigma_f >=< \phi >< \Sigma_f >$$

This is the case as long the two variables are not correlated — i.e. their correlation coefficient is $\rho = 0$. In reality, given the limited number of batches, one should aim at a correlation coefficient of the sampled random variables $\rho_s \rightarrow 0$. The sample correlation coefficient will be the more representative of reality the better

the statistics, meaning more batches imply ρ_s closer to 0. This discussion holds for the simplified case where single steps are considered for the depletion and no predictor-corrector scheme is implemented.

This explains why there is a discrepancy in the predicted ^{148}Nd concentration at discharge when comparing the simplified and the accurate models, which is reflective of a burnup difference among the simulations, being ^{148}Nd a burnup indicator. An overestimation of the burnup of the same relative order of magnitude — approximately 2% — was found in the models of Calvert Cliffs MKP109-P and Takahama SF95-4 (Figs. 3.43.12); this is not further investigated. The simplifications on the model of Gösgen GU3 (Fig. 3.8) result in an underestimation which might as well be due to a different effect of the simplifications on that more complex model.

Appendix B

Final inventory of the analysed samples

As reported in Fig. B.1, calculations with four different nuclear data libraries were performed. The considered nuclear data libraries were ENDF/B-VIII.0 [4], ENDF/B-VII.1 [41], JEFF-3.1.2 [5], JEFF-3.3 [42]. The differences among the results obtained in the four simulations are due to the different nuclear data evaluation given in the different libraries. The choice of the libraries also allows one to see how the library evolution through the years affects the results in a PWR irradiation context.

The changes are relatively small among the nuclear data libraries on the considered set of nuclides of interest for the SNF observables.

The concentrations of the analysed nuclides after cycle 18 are reported in Fig. B.2 The inventory is reported in logarithmic scale to enable comparison of the different order of magnitude of concentration of the different nuclides.

The discharge predicted sample inventory for Takahama SF95-4 is reported in Fig. B.3. The nuclides presented and their relevance for the SNF observables are reported in Tab. 1.2.

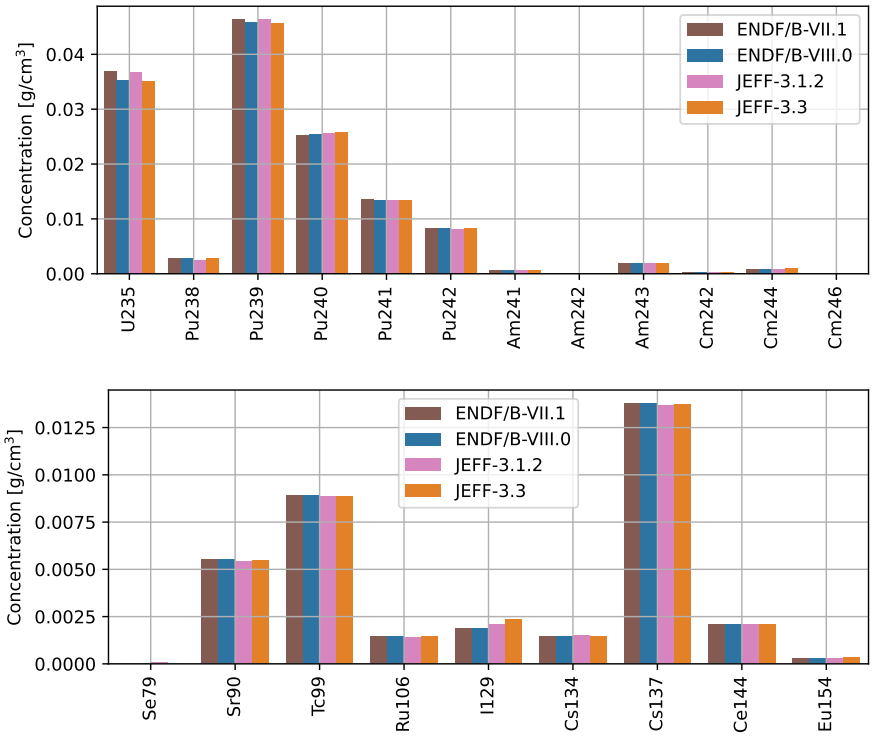

Figure B.1: Calvert Cliffs MKP109-P: Sample nuclide content after irradiation cycle 5. ^{238}U not included for the sake of visualisation. ^{238}U concentration after irradiation was computed to be approximately 8.27 $\frac{\text{g}}{\text{cm}^2}$ with a standard deviation close to 0.01% among the different nuclear data libraries, which show almost complete agreement.

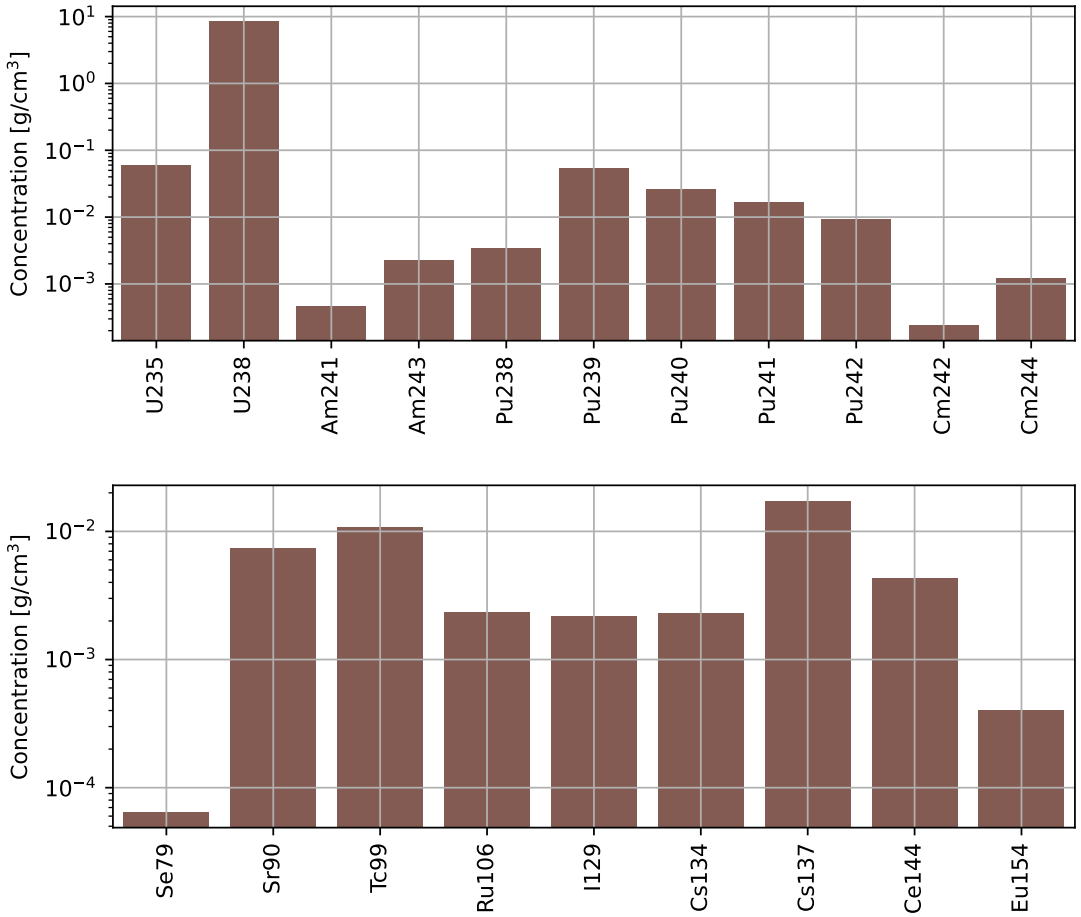

Figure B.2: Gösgen GU3: Sample inventory after irradiation cycle 18.

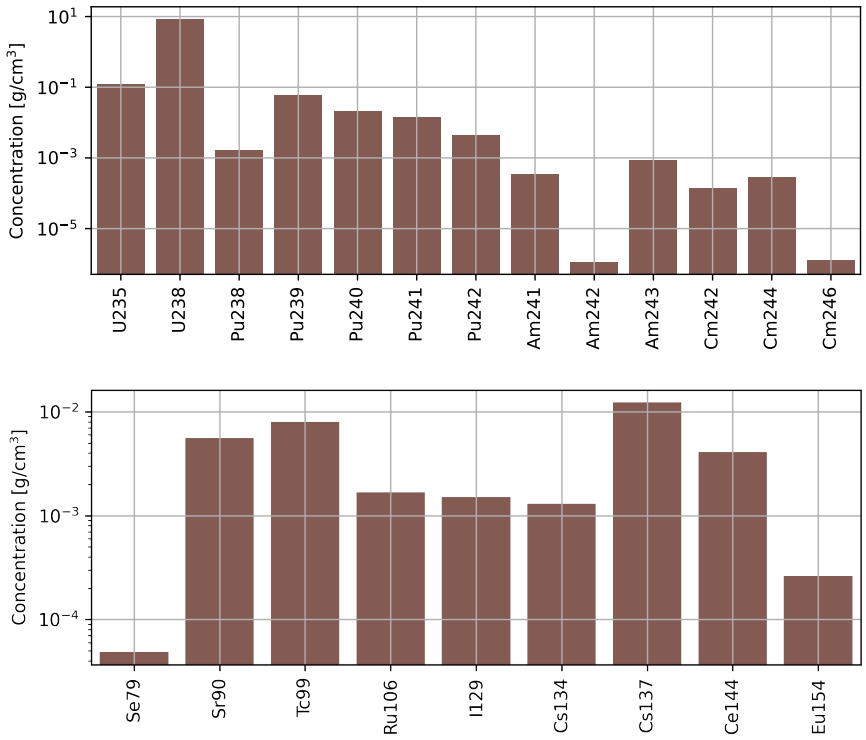

Figure B.3: Takahama SF95-4: Sample nuclide content after irradiation.

Bibliography

[1] IEA. *World Energy Outlook 2021*. IEA Publications, 2021. URL: www.iea.org/weo (cit. on pp. ii, 1).

[2] Agence Nationale, Pour La, and Gestion D E S Dechets. *European Joint Programme on Radioactive Waste Management Periodic Reporting for period 2 - EURAD (European Joint Programme on Radioactive Waste Management)*. Tech. rep. 2019, pp. 1–5. DOI: 10.3030/847593. URL: https://cordis.europa.eu/project/id/847593 (cit. on pp. ii, 1, 3, 26, 35).

[3] *CHANDA project*. URL: http://www.chanda-nd.eu/ (visited on 07/17/2022) (cit. on pp. ii, 1).

[4] D.A. Brown et al. «ENDF/B-VIII.0: The 8 th Major Release of the Nuclear Reaction Data Library with CIELO-project Cross Sections, New Standards and Thermal Scattering Data». In: *Nuclear Data Sheets* 148 (Feb. 2018), pp. 1–142. ISSN: 00903752. DOI: 10.1016/j.nds.2018.02.001. URL: https://linkinghub.elsevier.com/retrieve/pii/S0090375218300206 (cit. on pp. ii, 18, 53, 72).

[5] A. J. Koning et al. «Status of the JEFF Nuclear Data Library». In: *Journal of the Korean Physical Society* 59.2(3) (Aug. 2011), pp. 1057–1062. ISSN: 0374-4884. DOI: 10.3938/jkps.59.1057. URL: http://www.jkps.or.kr/journal/DOIx.php?id=10.3938/jkps.59.1057 (cit. on pp. ii, 18, 72).

[6] K. Shibata et al. «JENDL-4.0: A New Library for Nuclear Science and Engineering». In: *Journal of Nuclear Science and Technology* 48.1 (Jan. 2011), pp. 1–30. ISSN: 0022-3131. DOI: 10.1080/18811248.2011.9711675. URL: https://www.tandfonline.com/doi/full/10.1080/18811248.2011.9711675 (cit. on pp. ii, 18).

[7] *Joint Evaluated Fission and Fusion (JEFF) Nuclear Data Library - JEFF-4T1 (TEST Library)*. URL: https://www.oecd-nea.org/dbdata/jeff/jeff40/t1/ (visited on 07/17/2022) (cit. on pp. ii, 18).

[8] L. Fiorito, G. Žerovnik, A. Stankovskiy, G. Van den Eynde, and P.E. Labeau. «Nuclear data uncertainty propagation to integral responses using SANDY». In: *Annals of Nuclear Energy* 101 (Mar. 2017), pp. 359–366. ISSN: 03064549. DOI: 10.1016/j.anucene.2016.11.026. URL: https://linkinghub.elsevier.com/retrieve/pii/S0306454916305278 (cit. on pp. ii, 20).

[9] Nuclear Power Estimates. *REFERENCE DATA SERIES No. 1 2012 Edition*. 1. 2012. ISBN: 9789201244215 (cit. on p. 1).

[10] IAEA; OECD; NEA. *Back End of the Nuclear Fuel Cycle: Strategies and Options*. 1987. ISBN: 9200501877 (cit. on p. 2).

[11] V. T. Sorokin and D. I. Pavlov. «THE COST OF RADWASTE DISPOSAL: FOREIGN ASSESSMENTS». In: *Radioactive Waste* 1.6 (2019), pp. 39–46. URL: http://eng.radwaste-journal.ru/docs/journals/6/the_cost_of_radwaste_disposal.pdf (cit. on p. 2).

[12] G. Ilas, I. C. Gauld, and B.D Murphy. *Protecting People and the Environment Analysis of Experimental Data for High Burnup PWR Spent Fuel Isotopic Validation-ARIANE and REBUS Programs (UO_2 Fuel) Office of Nuclear Regulatory Research*. Tech. rep. Oak Ridge National Laboratory, Feb. 2010. URL: www.ntis.gov (cit. on pp. 3, 24).

[13] G. Ilas and I. Gauld. *Analysis of Experimental Data for High Burnup PWR Spent Fuel Isotopic Validation - Vandellos II Reactor*. Tech. rep. Oak Ridge, TN (United States): Oak Ridge National Laboratory (ORNL), Jan. 2011. DOI: 10.2172/1003739. URL: www.ansi.org%20https://www.osti.gov/servlets/purl/1003739/ (cit. on pp. 3, 25).

[14] J. Eysermans, M. Verwerft, K. Govers, R. Ichou, G. Ilas, U. Meryturek, N. Messaoudi, P. Romojaro, and N. Slosse. «REGAL International Program: Analysis of experimental data for depletion code validation». In: *Annals of Nuclear Energy* 172 (July 2022). ISSN: 18732100. DOI: 10.1016/J.ANUCENE.2022.109057 (cit. on pp. 3, 24).

[15] G. Žerovnik et al. *Observables of interest for the characterisation of Spent Nuclear Fuel*. Tech. rep. EC/JRC, 2018. DOI: 10.2760/418524. URL: https://op.europa.eu/s/oFdI (cit. on p. 4).

[16] B.L. Broadhead, M.D. DeHart, J.C. Ryman, J.S. Tang, and C.V. Parks. *Investigation of nuclide importance to functional requirements related to transport and long-term storage of LWR spent fuel*. Tech. rep. Oak Ridge, TN: Oak Ridge National Laboratory (ORNL), June 1995. DOI: 10.2172/95570. URL: http://www.osti.gov/servlets/purl/95570-DvhWEa/webviewable/ (cit. on p. 4).

[17] C. V. Parks, M. D. DeHart, and J. C. Wagner. *Review and Prioritization of Technical Issues Related to Burnup Credit for LWR Fuel*. Tech. rep. Oak Ridge, TN (United States): Oak Ridge National Laboratory (ORNL), Mar. 2000. DOI: 10.2172/814192. URL: http://www.osti.gov/servlets/purl/814192/ (cit. on p. 4).

[18] I. C. Gauld and J. C. Ryman. *Nuclide Importance to Criticality Safety, Decay Heating, and Source Terms Related to Transport and Interim Storage of High-Burnup LWR Fuel*. Tech. rep. Oak Ridge, TN (United States): Oak Ridge National Laboratory (ORNL), Dec. 2000. DOI: 10.2172/799527. URL: www.nrc.gov/NRC/ADAMS/index.html.%20http://www.osti.gov/servlets/purl/799527/ (cit. on p. 4).

[19] NEA/WPNCS/EGADSNF. *Spent Nuclear Fuel Assay Data for Isotopic Validation*. Tech. rep. 2011. URL: www.oecd-nea.org (cit. on pp. 4, 16).

[20] T. Haavisto. *Synthesis of Final Disposal Related Nuclides*. Tech. rep. April. 2014. URL: https://inis.iaea.org/collection/NCLCollectionStore/_Public/45/107/45107629.pdf (cit. on pp. 4, 23).

[21] I. C. Gauld and C. V. Parks. *Review of Technical Issues Related to Predicting Isotopic Compositions and Source Terms for High-Burnup LWR Fuel — NUREG/CR-6701 ORNL/TM-2000/277, ORNL/TM-2000/277 3*. Tech. rep. 2000, p. 94 (cit. on pp. 4, 23).

[22] D. Rochman, W. Zwermann, S. C. van der Marck, A. J. Koning, H. Sjöstrand, P. Helgesson, and B. Krzykacz-Hausmann. «Efficient Use of Monte Carlo: Uncertainty Propagation». In: *Nuclear Science and Engineering* 177.3 (July 2014), pp. 337–349. ISSN: 0029-5639. DOI: 10.13182/NSE13-32. URL: https://www.tandfonline.com/doi/full/10.13182/NSE13-32 (cit. on pp. 5, 13, 28).

[23] M. L. Williams, G. Ilas, W. J. Marshall, and B. T. Rearden. «Applications of nuclear data covariances to criticality safety and spent fuel characterization». In: *Nuclear Data Sheets* 118.1 (2014), pp. 341–345. ISSN: 00903752. DOI: 10.1016/j.nds.2014.04.075. URL: http://dx.doi.org/10.1016/j.nds.2014.04.075 (cit. on p. 5).

[24] C.J. Díez, O. Buss, A. Hoefer, D. Porsch, and O. Cabellos. «Comparison of nuclear data uncertainty propagation methodologies for PWR burn-up simulations». In: *Annals of Nuclear Energy* 77 (Mar. 2015), pp. 101–114. ISSN: 03064549. DOI: 10.1016/j.anucene.2014.10.022. arXiv: 1411.0834. URL: https://linkinghub.elsevier.com/retrieve/pii/S0306454914005611 (cit. on p. 5).

[25] L. Fiorito, D. Piedra, O. Cabellos, and C.J. Diez. «Inventory calculation and nuclear data uncertainty propagation on light water reactor fuel using ALEPH-2 and SCALE 6.2». In: *Annals of Nuclear Energy* 83 (Sept. 2015), pp. 137–146. ISSN: 03064549. DOI: 10.1016/j.anucene.2015.03.046. URL: https://linkinghub.elsevier.com/retrieve/pii/S0306454915002054 (cit. on pp. 5, 13, 28, 38).

[26] O. Leray, D. Rochman, P. Grimm, H. Ferroukhi, A. Vasiliev, M. Hursin, G. Perret, and A. Pautz. «Nuclear data uncertainty propagation on spent fuel nuclide compositions». In: *Annals of Nuclear Energy* 94 (Aug. 2016), pp. 603–611. ISSN: 03064549. DOI: 10.1016/j.anucene.2016.03.023. URL: https://linkinghub.elsevier.com/retrieve/pii/S0306454916301499 (cit. on p. 5).

[27] D. Rochman et al. «Nuclear Data Uncertainties for Typical LWR Fuel Assemblies and a Simple Reactor Core». In: *Nuclear Data Sheets* 139 (Jan. 2017), pp. 1–76. ISSN: 00903752. DOI: 10.1016/j.nds.2017.01.001. URL: https://linkinghub.elsevier.com/retrieve/pii/S0090375217300017 (cit. on p. 5).

[28] G. Ilas and H. Liljenfeldt. «Decay heat uncertainty for BWR used fuel due to modeling and nuclear data uncertainties». In: *Nuclear Engineering and Design* 319 (Aug. 2017), pp. 176–184. ISSN: 00295493. DOI: 10.1016/j.nucengdes.2017.05.009. URL: https://linkinghub.elsevier.com/retrieve/pii/S0029549317302376 (cit. on p. 5).

[29] C. Wemple and W. Zwermann. «Nuclear data uncertainty propagation by the XSUSA method in the HELIOS2 lattice code». In: *EPJ Web of Conferences* 146 (Sept. 2017). Ed. by A. Plompen, F.-J. Hambsch, P. Schillebeeckx, W. Mondelaers, J. Heyse, S. Kopecky, P. Siegler, and S. Oberstedt, p. 02020. ISSN: 2100-014X. DOI: 10.1051/epjconf/201714602020. URL: http://www.epj-conferences.org/10.1051/epjconf/201714602020 (cit. on p. 5).

[30] B. Ebiwonjumi, C. Kong, P. Zhang, A. Cherezov, and D. Lee. «Uncertainty quantification of PWR spent fuel due to nuclear data and modeling parameters». In: *Nuclear Engineering and Technology* 53.3 (Mar. 2021), pp. 715–731. ISSN: 17385733. DOI: 10.1016/j.net.2020.07.012. URL: https://linkinghub.elsevier.com/retrieve/pii/S1738573320303521 (cit. on p. 5).

[31] L. Fiorito, P. Romojaro, O. Cabellos, M. García-Hormigos, A. Hernandez-Solis, S. Sánchez-Fernández, A. Stankovskiy, G. Van den Eynde, and G. Žerovnik. «On the use of criticality and depletion benchmarks for verification of nuclear data». In: *Annals of Nuclear Energy* 161 (Oct. 2021), p. 108415. ISSN: 03064549. DOI: 10.1016/j.anucene.2021.108415. URL: https:

//linkinghub.elsevier.com/retrieve/pii/S0306454921002917 (cit. on pp. 5, 43, 52, 55).

[32] A. B. Smith, P. R. Fields, and J. H. Roberts. «Spontaneous Fission Neutron Spectrum of Cf^{252}». In: *Physical Review* 108.2 (Oct. 1957), pp. 411–413. ISSN: 0031-899X. DOI: 10.1103/PhysRev.108.411. URL: https://journals.aps.org/pr/abstract/10.1103/PhysRev.108.411%20https://link.aps.org/doi/10.1103/PhysRev.108.411 (cit. on p. 6).

[33] A. D. Vijaya and A. Kumar. «The neutron spectrum of Am-Be neutron sources». In: *Nuclear Instruments and Methods* 111.3 (Sept. 1973), pp. 435–440. ISSN: 0029-554X. DOI: 10.1016/0029-554X(73)90199-7. URL: https://www.sciencedirect.com/science/article/pii/0029554X73901997 (cit. on p. 6).

[34] G. I. Bell and S. Glasstone. *Nuclear Reactor Theory*. 450 West 33rd Street, New York, N.Y 10001: Van Nostrand Reinhold, Oct. 1970. URL: https://www.osti.gov/biblio/4074688 (cit. on p. 7).

[35] P. J. Turinsky. *Handbook of Nuclear Engineering*. Ed. by D. G. Cacuci. Vol. 2. Springer, 2010, pp. 1241–1313. ISBN: 978-0-387-98130-7. DOI: 10.1007/978-0-387-98149-9_10. URL: https://link.springer.com/content/pdf/10.1007/978-0-387-98149-9.pdf (cit. on p. 9).

[36] D. Rochman and C.M. Sciolla. «Nuclear data uncertianty propagation for a typical PWR fuel assembly with burnup». In: *Nuclear Engineering and Technology* 46.3 (June 2014), pp. 353–362. ISSN: 17385733. DOI: 10.5516/NET.01.2014.712. URL: https://linkinghub.elsevier.com/retrieve/pii/S1738573315301303 (cit. on p. 13).

[37] Y. Wang, M. Cui, J. Guo, J. Niu, Y. Wu, B. Liu, and F. Li. «Lognormal-Based Sampling for Fission Product Yields Uncertainty Propagation in Pebble-Bed HTGR». In: *Science and Technology of Nuclear Installations* 2020 (Sept. 2020), pp. 1–21. ISSN: 1687-6075. DOI: 10.1155/2020/8014521. URL: https://www.hindawi.com/journals/stni/2020/8014521/ (cit. on p. 13).

[38] G. Žerovnik, A. Trkov, D. L. Smith, and R. Capote. «Transformation of correlation coefficients between normal and lognormal distribution and implications for nuclear applications». In: *Nuclear Instruments and Methods in Physics Research Section A: Accelerators, Spectrometers, Detectors and Associated Equipment* 727 (Nov. 2013), pp. 33–39. ISSN: 01689002. DOI: 10.1016/j.nima.2013.06.025. URL: https://linkinghub.elsevier.com/retrieve/pii/S0168900213008450 (cit. on p. 13).

[39] D. A. Rochman and E. Bauge. «Fission yields and cross sections: correlated or not?» In: *EPJ Nuclear Sciences & Technologies* 7 (Mar. 2021), p. 5. ISSN: 2491-9292. DOI: 10.1051/epjn/2021005. URL: https://www.epj-n.org/articles/epjn/full_html/2021/01/epjn200021/epjn200021.html (cit. on pp. 13, 39).

[40] R.N. Bratton, K.N. Ivanov, M.A. Jessee, and W.A. Wieselquist. «Bias and uncertainty assessment of pressurized water reactor fuel isotopics using SCALE». In: *Proceedings of the International Conference on Physics of Reactors, PHYSOR 2014*. 2014 (cit. on pp. 16, 27).

[41] M.B. Chadwick et al. «ENDF/B-VII.1 Nuclear Data for Science and Technology: Cross Sections, Covariances, Fission Product Yields and Decay Data». In: *Nuclear Data Sheets* 112.12 (Dec. 2011), pp. 2887–2996. ISSN: 00903752. DOI: 10.1016/j.nds.2011.11.002. URL: https://linkinghub.elsevier.com/retrieve/pii/S009037521100113X (cit. on pp. 18, 72).

[42] A. J. M. Plompen et al. «The joint evaluated fission and fusion nuclear data library, JEFF-3.3». In: *The European Physical Journal A* 56.7 (July 2020), p. 181. ISSN: 1434-6001. DOI: 10.1140/epja/s10050-020-00141-9. URL: http://link.springer.com/10.1140/epja/s10050-020-00141-9 (cit. on pp. 18, 72).

[43] P. Baeten, A. Stankovskiy, G. Van Den Eynde, C. Trakas, P.-M. Demy, and L. Villatte. *ALEPH2-A general purpose Monte Carlo depletion code*. Tech. rep. URL: https://www.researchgate.net/publication/286740932 (cit. on p. 19).

[44] X-5 Monte Carlo Team. *MCNP–A General Monte Carlo N-Particle Transport Code, Version 5*. Vol. 1: Overvew and Theory. Los Alamos National Laboratory, 2008 (cit. on p. 19).

[45] J.-F. Martin, I. Hill, M. Fleming, and O. Buss. *Update on activities in the NEA Nuclear Science Committee relevant to the NCSP NCSP Technical Program Review*. 2022 (cit. on p. 20).

[46] J. Leppänen, M. Pusa, T. Viitanen, V. Valtavirta, and T. Kaltiaisenaho. «The Serpent Monte Carlo code: Status, development and applications in 2013». In: *Annals of Nuclear Energy* 82 (Aug. 2015), pp. 142–150. ISSN: 03064549. DOI: 10.1016/j.anucene.2014.08.024. URL: https://linkinghub.elsevier.com/retrieve/pii/S0306454914004095 (cit. on p. 20).

[47] G. Van Rossum and F. L. Drake Jr. *Python tutorial*. Centrum voor Wiskunde en Informatica Amsterdam, The Netherlands, 1995 (cit. on p. 20).

[48] M. Herman and A. Trkov. *ENDF-6 Formats Manual*. Tech. rep. National Nuclear Data Center Brookhaven National Laboratory Upton, NY, 2010. URL: www.nndc.bnl.gov (cit. on p. 20).

[49] R. Macfarlane, D. W. Muir, R. M. Boicourt, A. C. Kahler, III, and J. L. Conlin. *The NJOY Nuclear Data Processing System, Version 2016*. Tech. rep. Los Alamos, NM (United States): Los Alamos National Laboratory (LANL), Jan. 2017. DOI: 10.2172/1338791. URL: http://www.osti.gov/servlets/purl/1338791/ (cit. on pp. 21, 38).

[50] G. Žerovnik, A. Trkov, and I. A. Kodeli. «Correlated random sampling for multivariate normal and log-normal distributions». In: *Nuclear Instruments and Methods in Physics Research Section A: Accelerators, Spectrometers, Detectors and Associated Equipment* 690 (Oct. 2012), pp. 75–78. ISSN: 01689002. DOI: 10.1016/j.nima.2012.06.036. URL: https://linkinghub.elsevier.com/retrieve/pii/S0168900212007024 (cit. on p. 21).

[51] C. R. Harris et al. «Array programming with NumPy». In: *Nature* 585.7825 (Sept. 2020), pp. 357–362. ISSN: 14764687. DOI: 10.1038/S41586-020-2649-2. arXiv: 2006.10256 (cit. on p. 21).

[52] *GitHub*. 2020. URL: https://github.com/ (cit. on p. 21).

[53] E. Belfiore. «Sensitivity and uncertainty analysis for nuclear data in spent nuclear fuel characterization». Master's Thesis. Politecnico di Torino, Belgian Nuclear higher Education Network, 2022 (cit. on p. 22).

[54] F. Michel-Sendis et al. «SFCOMPO-2.0: An OECD NEA database of spent nuclear fuel isotopic assays, reactor design specifications, and operating data». In: *Annals of Nuclear Energy* 110 (Dec. 2017), pp. 779–788. ISSN: 03064549. DOI: 10.1016/j.anucene.2017.07.022. URL: https://linkinghub.elsevier.com/retrieve/pii/S0306454917302104 (cit. on pp. 22, 23).

[55] N. Soppera, M. Bossant, and E. Dupont. «JANIS 4: An Improved Version of the NEA Java-based Nuclear Data Information System». In: *Nuclear Data Sheets* 120 (June 2014), pp. 294–296. ISSN: 0090-3752. DOI: 10.1016/J.NDS.2014.07.071 (cit. on p. 22).

[56] W. McKinney. «Data Structures for Statistical Computing in Python». In: *Proceedings of the 9th Python in Science Conference*. Ed. by Stéfan van der Walt and Jarrod Millman. 2010, pp. 56–61. DOI: 10.25080/Majora-92bf1922-00a. URL: https://conference.scipy.org/proceedings/scipy2010/mckinney.html (cit. on p. 23).

[57] The Pandas development Team. *pandas-dev/pandas: Pandas*. 2020. DOI: 10.5281/zenodo.3509134. URL: https://doi.org/10.5281/zenodo.3509134 (cit. on p. 23).

[58] M. Tarvainen, F. Lévai, T. E. Valentine, M. Abhold, and B. Moran. *NDA techniques for spent fuel verification and radiation monitoring Report on Activities 6a and 6b of Task JNT C799 (SAGOR) Finnish Support Programme to the IAEA Safeguards*. Helsinki: Oy Edita Ab, 1997. ISBN: 9517122225 (cit. on p. 23).

[59] J. W. Roddy, H. C. Claiborne, and R. C. Ashline. *Physical and Decay Characteristics of Commercial LWR Spent Fuel*. Tech. rep. 1986 (cit. on p. 25).

[60] G. Ilas, I. C. Gauld, F. C. Difilippo, and M. B. Emmett. *Analysis of Experimental Data for High Burnup PWR Spent Fuel Isotopic Validation -Calvert Cliffs, Takahama, and Three Mile Island Reactors*. Tech. rep. 2010. URL: www.ntis.gov (cit. on pp. 25, 35).

[61] F. Grimaldi, L. Fiorito, P. Romojaro, and A. Hernandez-Solis. «Nuclear data uncertainty quantification for the nuclide inventory of a Calvert Cliffs spent fuel sample». In: *International Conference on Physics of Reactors 2022 (PHYSOR 2022)*. 2022 (cit. on pp. 25, 27, 41).

[62] J. Hu, J.M. Giaquinto, I.C. Gauld, G. Ilas, and T.J. Keever. «Analysis of new measurements of Calvert Cliffs spent fuel samples using SCALE 6.2». In: *Annals of Nuclear Energy* 106 (Aug. 2017), pp. 221–234. ISSN: 03064549. DOI: 10.1016/j.anucene.2017.04.005. URL: https://linkinghub.elsevier.com/retrieve/pii/S0306454917300865 (cit. on pp. 25, 27).

[63] S.R. Pati and P.A. Van Saun. *Isotopic and transuranic nuclide content of three- and four- cycle Calvert Cliffs-I fuel — Research Project 1755-1, Final Report*. Tech. rep. Combustion Engineering, Inc., 1982 (cit. on p. 25).

[64] G. Radulescu, I. C. Gauld, and G. Ilas. *SCALE 5.1 Predictions of PWR Spent Nuclear Fuel Isotopic Compositions*. Tech. rep. Oak Ridge, TN (United States): Oak Ridge National Laboratory (ORNL), Mar. 2010. DOI: 10.2172/983556. URL: http://www.osti.gov/servlets/purl/983556/ (cit. on p. 25).

[65] R.J. Guenther, D.E. Blahnik, U.P. Jenquin, J.E. Mendel, L.E. Thomas, and C.K. Thornhill. *Characterization of spent fuel approved testing material–ATM-104*. Tech. rep. Richland, WA: Pacific Northwest National Laboratory (PNNL), Dec. 1991, pp. 1.1–8.52. DOI: 10.2172/138327. URL: http://www.osti.gov/servlets/purl/138327-9eLrcl/ (cit. on p. 25).

[66] S.R. Bierman and R.J. Talbert. *Benchmark data for validating irradiated fuel compositions used in criticality calculations*. Tech. rep. Richland, WA: Pacific Northwest National Laboratory (PNNL), Oct. 1994. DOI: 10.2172/10193492. URL: http://www.osti.gov/servlets/purl/10193492-BtkzI2/webviewable/ (cit. on p. 26).

[67] O. W. Hermann, S. M. Bowman, C. V. Parks, and M. C. Brady. *Validation of the scale system for PWR spent fuel isotopic composition analyses*. Tech. rep. Oak Ridge, TN (United States): Oak Ridge National Laboratory (ORNL), Mar. 1995. DOI: 10.2172/57886. URL: http://www.osti.gov/servlets/purl/57886/ (cit. on p. 27).

[68] D. Rochman, S.C. van der Marck, A.J. Koning, H. Sjöstrand, and W. Zwermann. «Uncertainty Propagation with Fast Monte Carlo Techniques». In: *Nuclear Data Sheets* 118.1 (Apr. 2014), pp. 367–369. ISSN: 00903752. DOI: 10.1016/j.nds.2014.04.082. URL: https://linkinghub.elsevier.com/retrieve/pii/S0090375214001124 (cit. on p. 28).

[69] C. Carmouze, R. Ichou, and L. Jutier. *Synthesis of the subgroup 7 activities: Specification of a benchmark on Sensitivity / Uncertainty Analysis for PWR UOx spent nuclear fuel*. Tech. rep. Working Party on Nuclear Criticality Safety (WPNCS), 2021 (cit. on pp. 30, 31).

[70] L. Pollet. «Validation of ALEPH2 burn-up code using benchmarks from SFCOMPO». Master's Thesis. Hasselt University, Katholieke Universiteit Leuven, 2021 (cit. on p. 30).

[71] Y. Nakahara, J. U. N. Inagawa, R. Nagaishi, S. Kurosawa, N. Kohno, M. Onuki, and H. Mochizuki. «Nuclide Composition Benchmark Data Set for Verifying Burnup Codes on Spent Light Water Reactor Fuels Management». In: *Nuclear Technology* 137 (2002), pp. 111–126 (cit. on p. 34).

[72] Yoshinori Nakahara, Kenya Suyama, and Takenori Suzaki. *Technical Development on Burn-up Credit for Spent LWR Fuels (Translation)*. Tech. rep. January. 2002 (cit. on p. 35).

[73] D. Rochman, M. Hursin, A. Vasiliev, and H. Ferroukhi. «Impact of H in H 2 O thermal scattering data on depletion calculation: k_∞ , nuclide inventory and decay heat». In: *EPJ Nuclear Sciences & Technologies* 7 (Dec. 2021), p. 24. ISSN: 2491-9292. DOI: 10.1051/epjn/2021027. URL: https://doi.org/10.1051/epjn/2021027%20https://www.epj-n.org/10.1051/epjn/2021027 (cit. on p. 38).

[74] P. Romojaro, K. Ambrožič, D. Čalič, L. Fiorito, and K. Govers. «Sensitivity and uncertainty analysis of PWR spent fuel observables to operational and model parameters». In: *International Conference on Physics of Reactors 2022 (PHYSOR 2022)*. 2022 (cit. on p. 39).

[75] R. Tuominen. *Doppler-broadening preprocessor routine*. URL: https://serpent.vtt.fi/mediawiki/index.php?title=Doppler-broadening_preprocessor_routine&oldid=5416 (visited on 08/08/2022) (cit. on p. 39).

[76] JEFF. *Nuclear Data Week - April 2022*. 2022. URL: https://www.oecd-nea.org/jcms/pl_66664/nuclear-data-week-april-2022 (visited on 07/17/2022) (cit. on p. 41).